Annu. Rev. Mater. Res. 2003. 33:289–319
doi: 10.1146/annurev.matsci.33.022702.155102

PROTON CONDUCTION MECHANISMS AT LOW DEGREES OF HYDRATION IN SULFONIC ACID–BASED POLYMER ELECTROLYTE MEMBRANES

S.J. Paddison
Computational Nanoscience Group, PSRL, Motorola Labs, Motorola Inc. 4200 W. Jemez Rd., Suite #300, Los Alamos, New Mexico 87544; email: sjpaddison@netscape.net

Key Words Nafion®, PEM, proton conduction, mechanism, sulfonic acid

■ **Abstract** The need to operate polymer electrolyte membrane (PEM) fuel cells at temperatures above 100°C, where the amount of water in the membrane is restricted, has provided much of the motivation for understanding the mechanisms of proton conduction at low degrees of hydration. Although experiments have not provided any direct information, numerous theoretical investigations have begun to provide the basis for understanding the mechanisms of proton conduction in these nano-phase-separated materials. Both the hydrated morphology and the nature of the confined water in the hydrophilic domains influence proton dissociation from the acidic sites (i.e., $–SO_3H$), transfer to the water environment, and transport through the membrane. The following molecular processes are discussed in connection to their role in the conduction of protons in sulfonic acid–based polymer electrolyte membranes (PEMs): (*a*) local chemistry of the hydrophilic side chains; its effect on the dissociation of the proton and eventual stabilization (separation) of the proton in the water; (*b*) the presence of neighboring sulfonic acid groups on proton transfer; and (*c*) the effect of the distribution of the sulfonate groups on the transport of protons in the channels/pores of the membrane.

INTRODUCTION

Successful integration of the polymer electrolyte membrane (PEM) fuel cell into the mass-market will come as a result of the development of novel materials that include improved and low-cost electrocatalysts for the fuel and air electrodes, and membranes exhibiting high-proton conductivity with minimal (or perhaps no) water (1). These new materials, possessing improved properties, will emerge as a result of a collaborative effort between experimentalists, engineers, and theorists, the latter doing both device and materials modeling. For physical and chemical modeling to play a role in the suggestion of new materials the modeling must be at the nano- and even molecular scale, and ideally it should not be phenomenological but rather from first principles. This review focuses on what is known (from

both experiments and ab initio modeling) concerning the mechanisms of proton conduction in sulfonic acid–based PEMs, and specifically, these membranes at low degrees of hydration.

FUNCTION OF THE PEM

The function of the PEM in a fuel cell is to effectively separate the anode and cathode electrodes and to facilitate the conduction of protons. Thus the membrane serves as the electrolyte and completes the electrical circuit in the fuel cell. The first requirement implies that the membrane must possess chemical, thermal, and morphological stability and little or no gas permeability over a variety of operating conditions. With respect to the second requirement, proton conduction in most PEMs is directly linked to the degree of hydration of the membrane. As the fuel cell is an open system with different sinks and sources for water, the chemical state and transport properties of both the water and the protonic charge carriers have to be known and to fall within defined values. These depend on the actual operating conditions such as temperature, choice of fuel, gas humidification and gas flow, properties of the membrane/electrode interfaces, transport within the gas diffusion electrode, and electrical current drained from the fuel cell. The relevant membrane properties may be summarized as follows: (*a*) the relationship between the concentration and activity of the water (hydration isotherms and swelling in liquid water); (*b*) the dependence of the proton conductivity, water diffusion coefficient, electroosmotic drag of water, and water permeability on the degree of hydration of the membrane; and (*c*) the elastic properties of the membrane. These parameters determine the water concentration profiles and the dependent properties (such as the overall proton conductivity) for given boundary conditions.

THE TYPES OF WATER-DEPENDENT PEMs

Because of its favorable chemical, mechanical, and thermal properties along with high protonic conductivity when sufficiently hydrated, the perfluorinated sulfonic acid ionomer membrane Nafion® (a DuPont registered trademark polymer) is the prototypical PEM for fuel cell applications. There are, however, several drawbacks to the practical use of Nafion that include cost, maximum operating temperature ($<90^{\circ}$C), and problems associated with the transport of water (i.e., electroosmotic drag) and fuel (e.g., methanol). This has driven a number of strategies into the design of alternative materials (2).

Although many of the novel membranes are also sulfonated polymers, membranes with sulfonimide functionals are also under investigation for improved thermal stability and proton conductivity (3, 4). These imides, however, are faced with limitations similar to those of the fluorinated sulfonic acid–based polymers in terms of cost and water and methanol crossover.

Distinctly different efforts into the design of advanced and cost-effective membranes include (*a*) sulfonated aromatic backbone polymers, i.e., polyetherketones (PEEKK, PEEK, etc.) (5–7); (*b*) the inclusion of small inorganic particles such as silica (8–10) or zirconium phosphates and sulfophenylphosphates (10) within the membrane; (*c*) acid/base blending or covalent cross-linking of polymers (11, 12); and (*d*) the complexation of basic polymers (e.g., polybenzimidazole) with oxoacids (13, 14) (e.g., phosphoric acid) (15).

The PEEKK membranes offer definite cost and stability advantages over Nafion membranes but exhibit substantially lower conductivity at the lower water contents. The membranes in (*b*) and (*c*) exhibit increased thermal stability (up to 140°C) and reduced swelling and methanol and water crossover, but at a penalty in terms of conductivity and mechanical stability. Finally, the membranes with immobilized acid demonstrate conductivities as high as those seen in the hydrated systems (16) but with drastically reduced methanol crossover (17).

There are several significant advantages for PEM fuel cell operation at temperatures above 100°C. Both electro-catalytic and -transport phenomena are significantly enhanced in this temperature range. The improvement in electro-catalysis could lead to the reduction or even elimination of precious metal catalysts. Also, for PEM fuel cells operating on reformed fuels, or as direct methanol fuel cells (DMFCs), problems associated with adsorbed impurities and intermediates are substantially alleviated. Drawbacks to operation in this temperature range include questions regarding membrane stability and the need to pressurize the feed stream to maintain the water content of the membrane necessary to allow sufficient proton conduction. Maintenance of the water content, interestingly, also could be an important contributor to membrane stability because dissociation of the extremely strong sulfonic acid moiety levels the acidity of that group.

Thus there is substantial interest in the development of membranes that exhibit high proton conductivity at low degrees of hydration. Clearly, the route to these PEMs will come as the result of solid fundamental understanding of proton conduction in existing materials.

MORPHOLOGY OF THE PEMs

A great number of experimental techniques have been applied in an effort to understand both the morphology and ion distribution of PEMs and the correlation of these two properties. These techniques include small- (6, 18–23) and wide- (24, 25) angle X-ray scattering, neutron scattering (22, 26, 27), differential scanning calorimetry (28–31), dielectric relaxation (32–35), dielectric spectroscopy (36, 37), transmission (38–40) and scanning (41) electron microscopy, atomic force microscopy (42–44), scanning electrochemical microscopy (45), NMR (6, 46–52) and ESR (53, 54) spectroscopy, IR (31, 55, 56) and Raman (57) spectroscopy, Mossbauer spectroscopy (58, 59), fluorescence probe studies (60–63), and ac impedance investigations (64, 65).

Despite the substantial work in the characterization of PEMs, many performance features remain incompletely understood. This is largely due to the very inhomogeneous nature of these membranes when hydrated. Nevertheless, a definite correlation exists between the transport of protons and water and the hydrated morphology of the sulfonic acid–based ionomers. Sulfonated polymers naturally combine, in one macromolecule, the high hydrophobicity of the backbone with the high hydrophilicity of the sulfonic acid functional groups. In the presence of water, this gives rise to nano-separation of hydrophobic/hydrophilic domains. The sulfonic acid functional groups aggregate to form hydrophilic domains that are hydrated in the presence of water. Whereas the connected hydrophilic domain is responsible for the transport of protons and water, the hydrophobic domain provides the polymer with the morphological stability and prevents the polymer from dissolving in water.

Although the integrity and structural stability of the Nafion membrane is provided for by the polytetrafluoroethylene (PTFE) backbones, it is the hydrophilic ionic clusters that facilitate the transport of ions and water in the membrane. The microstructure of these clusters or pores consists of an interfacial region of solvated perfluoroether side chains ($-OCF_2CF(CF_3)OCF_2CF_2SO_3^-$) separating the polymer matrix from more bulk-like water in the pores. The dimensions and shape of the clusters with the uptake of water are determined by the equilibrium reached between the internal osmotic pressure of the clusters and the counteracting elasticity of the organic matrix (66). The nature and character of the water in the pores, however, are not well characterized (discussed below).

During the early efforts to understand the morphology of Nafion, a model was proposed by Gierke et al. (24, 67, 68) suggesting that the clusters were inverted micellar spheres with diameters ranging from 40 to 50 Å, interconnected by channels with a diameter and length of 10–20 Å. Their interpretation of X-ray scattering data led them to conclude that the pores contained approximately 70 side chains and 1000 water molecules. Although their model gained fairly wide acceptance, the experimental investigations of others have since indicated that the spherical shape and uniform spacing of the pores are serious oversimplifications. It should also be realized that there is no direct experimental evidence for the channels connecting the clusters in Gierke's model.

Falk (56) concluded from an infrared study that the hydrated clusters are highly nonspherical in shape, with a significant amount of water in the clusters associated with the fluorocarbon phase (the interfacial component of the pores). Additional X-ray diffraction and differential scanning calorimetry measurements by Starkweather (70) led him to propose a lamellar hexagonal structure of the fluorocarbon backbones with the side chains extending perpendicular to the alignment of the PTFE backbones and into ionic cluster domains. More recently, Litt (71), through reexamination of the data of Gierke, proposed a lamellar morphology for Nafion where the side chains are located in large surface area domains planar to one another. With hydration of the membrane, the water simply collects in the ionic domains (clusters) pushing the nonpolar domains (PTFE backbones) further apart subject to restraint by tie molecules. Similar lamellar micelle structures

were observed by Rebrov et al. (72) for Nafion solubilized in DMF and by Zoppi et al. (41) for Nafion with incorporated silicon oxide. The lamellar geometry in the separation of the two phases was also witnessed in a recent modeling study by Krueger and colleagues (73, 74) using a lattice-based self-consistent mean field theory (SCMF) approach.

From a combined differential scanning calorimetry and FTIR study on cast Nafion films, Zanderighi et al. (31) concluded that a continuous water phase exists only when the relative humidity of the membrane exceeds 90%. Their conclusion is in contrast to the results of a recent and elegant modeling investigation of the morphology of hydrated Nafion by Khalatur et al. (75). Using a hybrid Monte Carlo/reference interaction site model (MC/RISM) simulation technique, with potentials of mean force fitted from semiempirical AM1 molecular orbital calculations of Nafion fragments, they concluded that (*a*) the aggregation processes for the sulfonic acid groups were intensified even with a small amount of water in the membrane; (*b*) the water formed specific cage-like structures similar to clathrates; and (*c*) the geometries in (*b*) were favorable to the formation of continuous channels at very low hydration and even almost dry membranes. This latter point is certainly consistent with the measurement of reasonable conductivities in Nafion membranes with very little water present (i.e., as low as 1 H_2O/SO_3H) (49).

The very recent high-intensity, small-angle X-ray scattering (SAXS) and small-angle neutron scattering (SANS) investigations of Gebel et al. (22, 23) for Nafion membranes in different swelling states have given a slightly different picture to the morphology. Their results suggest aggregation of the ionomer chains into elongated PTFE bundles with diameters of about 40 Å and lengths greater than 100 nm surrounded by the sulfonate groups and water molecules. In addition, their detailed analysis of the high-resolution SAXS data and the evolution of characteristic spacing with the water/polymer ratio suggests structural features even on the nano-scale. Relative to the conclusions of the work described above, this is essentially an inversion in the microstructure (i.e., hydrophobic material surrounded by hydrophilic domains).

Undoubtedly the most self-consistent picture for the morphology of sulfonic acid polymers has been put forth by Kreuer (6) and Ise (76). Their conclusions are based on a thorough and careful analysis of results from SAXS experiments, pulsed-field-gradient (PFG)-NMR measurements, and on broadband dielectric spectroscopy of Paddison et al. (36, 37) all performed on both Nafion and sulfonated PEEKK membranes over a range of hydration levels. A pictorial representation of their results is presented in Figure 1.

Their SAXS experiments revealed a shifted (toward higher scattering angles) and broadened ionomer peak, and a higher scattering intensity in the Porod-regime for the PEEKK membranes compared with Nafion membranes. These results were interpreted to infer smaller characteristic separation lengths with a wider distribution and a larger internal interface between the hydrophobic and hydrophilic domains for the aromatic versus the perfluoro-polymers. This picture is consistent with the following facts: (*a*) In the PEEKK membranes there is a smaller hydrophilic/hydrophobic difference (the aromatic backbone is less hydrophobic

than PTFE, and the sulfonic acid functional group is less acidic and therefore also less polar) (see below). (*b*) There is also less flexibility in the aromatic backbone. These results naturally lead to the conclusion that the separation into hydrophilic and hydrophobic domains is less pronounced for the sulfonated PEEKK membranes compared with the Nafion membranes. The SAXS data were also used with water self-diffusion coefficients derived from (PFG)-NMR to parameterize a simple yet self-consistent model for the microstructure, based on an assumed cubic hydrophilic channel system in the hydrophobic medium. For Nafion, the microstructure was represented by low-dimensional polymeric objects (i.e., channels or pores) forming the spaces filled with water. Although this analysis did not give any information on long-range percolation, estimates of channel diameter, channel separation, degree of branching, and the number of dead-end channels were obtained for both types of polymers. As illustrated in Figure 1, the water-filled channels in sulfonated (S-) PEEKK are narrower than those in Nafion. They are less separated and more branched with more dead-end pockets. These features correspond to the larger hydrophilic/hydrophobic interface and, therefore, also to a larger average separation of neighboring sulfonic acid functional groups.

From the above discussion it should be obvious that the hydrated morphology and the shape of the domains have not (and probably can not) been determined with absolute certainty from only these experiments, and yet there is a clear correlation between the hydrated morphology and the conduction of protons in these systems. In the next section the properties of the water in a PEM are discussed.

THE NATURE OF THE WATER IN PEMs

In hydrated PEMs, water and protons are confined to domains with dimensions of only nanometers. Because the water is confined, its structural and dynamical properties are distinct from bulk water, a trend that becomes even more significant as the water content is decreased and the density of anionic groups increased. Thus the state or nature of the water has direct consequences on the transport properties (dissociation, transfer, and transport) of the protons within the membranes.

There are many situations in nature where water is confined to very small (even nanodimensional) regions. These include water in sandstones, in biological cells, on the surface of proteins, and, of relevance to this review, in hydrated ionomer membranes. This, in part, explains the increasing number of experimental and theoretical studies aimed at understanding the structural and dynamical properties of the water in these environments, along with the consequent effects on ion mobility and selectivity (77–83).

In attempting to elucidate the connection between the hydration state and the nature of the water in the membrane, Paddison et al. (36, 37) measured the microwave region (0.045–30 GHz) of the dielectric spectrum of both Nafion (105, 117, and 120) and PEEK (L540, G530, and a blend with 5% PES) membranes. Their choice to conduct measurements with an electric field with frequency as high as 30 GHz was based on the observation that the principal absorption band attributed to a Debye-type relaxation of molecular origin in pure bulk water occurs at about

18 GHz. In addition to obtaining the dielectric constant of these membranes as a function of both water content and frequency (the latter being a difficult quantity to obtain over such a broad range), they also computed conductivities; the latter showing good agreement with measurements from others. Their results showed a strong dependence in the dielectric constant and loss factor in the Nafion membranes with water content, but a much weaker dependence in the PEEK membranes. These results are completely consistent with the morphologies derived by Kreuer (6) and Ise (76) from SAXS and (PFG)-NMR experiments (see above), where owing to the stronger confinement of water in the narrow channels of the PEEK membranes, the dielectric constant is lower (i.e., the water molecules are more tightly bound, to each other and to the fixed sulfonate groups). Similar conclusions were also reached by MacMillan et al. (52) in proton and deuterium NMR measurements of hydrated Nafion, where the reorientational correlation times of the water were found to scale as a function of the pore diameter. The drawback or limitation in such experiments is that the results reflect only the dielectric response of the bulk material (i.e., both the polymer and the water) and thus specific information concerning only the water in the pores is somewhat obscured.

In an effort to quantify the state of the water in the nanopores of hydrated PEMs on a more microscopic level, Paul & Paddison (84–86) recently derived statistical thermodynamic models for the dielectric saturation of the water from the electrostatic fields produced by the fixed anionic groups (i.e., $-SO_3^-$). Their work follows in the spirit of the much earlier pioneering work of Booth (87). They assume that the field-dependent permittivity of the water, $\varepsilon(\mathbf{E})$, may be expressed as the sum of two terms according to

$$\varepsilon(\mathbf{E}) = n^2 + \frac{4\pi P(\mathbf{E})}{\varepsilon_0 E}, \qquad 1.$$

where n is the refractive index, and E and P are the magnitudes of the electric field, $\mathbf{E}$, and polarization $\mathbf{P}$, respectively. The polarization is computed from a realization that it is a functional derivative of the Helmholtz energy, A, i.e.,

$$\mathbf{P}(\mathbf{r}, \mathbf{E}, \mathbf{E}_e) = -\delta A(\mathbf{E}, \mathbf{E}_e)/\delta \mathbf{E}_e(\mathbf{r}), \qquad 2.$$

where the dependence of both the polarization and the energy on the electrostatic field due to the fixed anionic groups, $\mathbf{E}$, and an external probing electric field, $\mathbf{E}_e$, are explicitly declared. One of the important implications of Equation 2 is the inclusion of the electrostatic field as part of the total energy (Hamiltonian) of the system. Using the methods of statistical thermodynamics [see specifically References (85, 86) for details] and the assumptions of a cylindrical PEM pore with an axial periodic and radially symmetric distribution of point charges (for the fixed $-SO_3^-$ groups), Paul & Paddison calculated the radial profiles of the relative permittivity for Nafion and PEEKK membranes at various degrees of hydration. The most recent results for the dielectric constant as a function of radial position for Nafion membranes with water contents of $\lambda = 6$, 13, and 22.5 (these are the number of water molecules per sulfonic acid group) are plotted in Figure 2. These

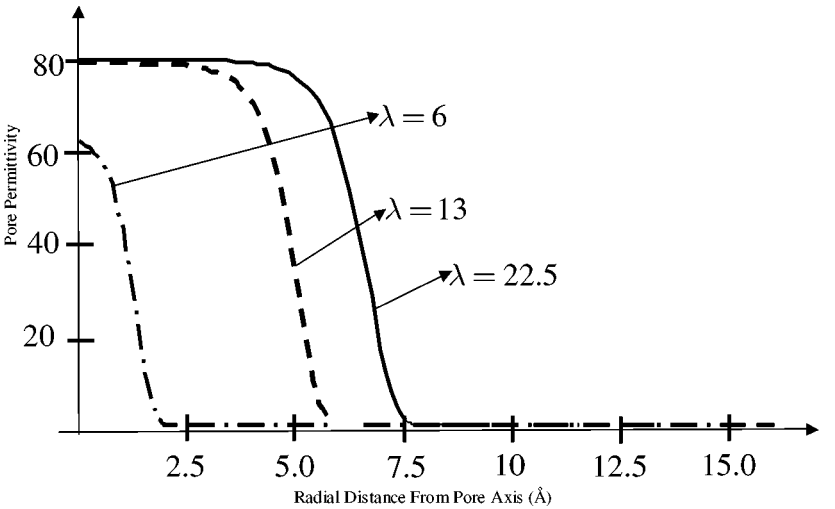

Figure 2 Computed radial dependence of the relative permittivity of the water in the pores of Nafion membranes with hydration levels (λ) of 6, 13, and 22.5 water molecules per sulfonic acid group. It is important to note that in the membrane at the lowest degree of hydration even the water in the center of the pore has a dielectric constant substantially lower than that of bulk water.

water contents were chosen because they represent a practical range of hydration for an operating fuel cell. Important findings from these calculations include (*a*) the permittivity of the water in the center of the pore at the lowest water content is only about 70% of that of bulk water ($\varepsilon = 80$); (*b*) the permittivity of the water in the center of the pores at the higher two water contents reaches that of bulk water; and (*c*) for the fully hydrated membrane $\lambda = 22.5$, there is a central region in the pore (one third of the pore radius $\approx$6 Å) where the water has a permittivity of bulk water. All of these plots show an ordering in the water (as witnessed in a reduction in dielectric constant) that occurs when one approaches the first two monolayers (i.e., the first and second hydration shells) of water around the fixed anionic sites. These results show a qualitative agreement with the molecular dynamics simulation results of Senapati & Chandra (81) for water confined in spherical nanocavities (i.e., the magnitude of the dielectric constant increasing with the diameter of the cavity) and the results of Gutman et al. (88–91) for water in the microcavities in proteins and phospholipid structures.

MECHANISMS OF PROTON CONDUCTION

In reviewing the work done toward determining the mechanisms of proton conduction in hydrated PEMs, it is insightful to begin a discussion of what is known concerning the diffusion of protons in bulk water. We know that with sufficient

hydration (and certainly for PEMs that are fully hydrated) the membrane contains a water phase that is similar in character to bulk water (as assessed by its dielectric properties).

Proton Diffusion in Bulk Water

Our present understanding concerning the transfer (short- and long-range) of protons in bulk water comes primarily from the quantitative evaluations of Agmon (92, 93) and Kreuer (94, 95) and from state-of-the-art ab initio molecular dynamics simulations of Tuckerman et al. (96–98) and Marx et al. (99, 100). Collectively, their work dispels many of the inconsistent and contradictory explanations that have been presented in the literature and provides a solid fundamental explanation for the anomalously high mobility of protons in liquid water. Having said that, the actual mechanism is still highly contentious. Nevertheless, the understanding gleaned from their analyses concerning proton conduction in bulk water is presented here.

Figure 3 illustrates the important species and features involved in the diffusion of an excess proton in bulk water, along with the timescales for the transfer of the proton between two limiting structures. These two stable forms of the hydrated proton depicted in the illustration are the Zundel ion ($H_5O_2^+$) and the Eigen ion, a hydrated hydronium ion ($H_9O_2^+$). The hydrogen bond distance (i.e., O–O) in the Zundel ion is only about 2.5 Å, significantly shorter than the average hydrogen bond length in bulk water (≈2.8 Å), whereas the length of the hydrogen bonds in the Eigen ion is slightly less contracted (≈2.6 Å). In bulk water the Eigen ion is slightly less favorable than the Zundel ion, suggesting that a structure with fewer but shorter hydrogen bonds is preferred in the vicinity of the excess proton (95). Although a number of other intermediates exist, the system exists as either a $H_5O_2^+$ or a $H_9O_2^+$ for the majority of the time, with rapid fluctuations between the two (i.e., $\sim 10^{-13}$ s). This is in contrast to the much slower transitions between the two Zundel ions depicted in Figure 3 ($\sim 10^{-12}$ s). In understanding the overall process of proton transport, it is important to realize that (*a*) the protonic charge follows the center of symmetry of the hydrogen bond pattern; (*b*) bond breaking and forming (reorientation) occurs in the weakly bound part of each complex; (*c*) proton transfer takes place in the contracted central part of each complex (indicated in blue in Figure 3); and (*d*) there is a strong coupling of both (*b*) and (*c*).

Proton Conduction in PEMs

The proton conduction mechanisms in hydrated PEMs may be understood from a consideration of dissociation of the proton from the acidic site, subsequent transfer of the proton to the aqueous medium, screening by water of the hydrated proton from the conjugate base (e.g., the sulfonate anion), and finally diffusion of the proton in the confined water within the polymer matrix. The discussion that follows addresses these processes individually.

Proton Dissociation

In an effort to obtain molecular-scale information concerning the effects of structure and local chemistry on the dissociation of protons in the acidic (and hydrophilic) sites in PEMs, Paddison et al. (101–109) embarked on a series of state-of-the-art, first-principles-based electronic structure calculations (see below). Due to the virtual impossibility of treating an entire ionomer in an ab initio manner and the fact that empirical or semiempirical methods, while computationally less demanding, give conformational results for the polymer interacting with water that are often grossly incorrect, only the polymeric subunits involved in the interaction with water were subjected to a full electron treatment.

In the electronic structure calculations reported by Paddison et al., minimum energy conformations of the hydrophilic portion (closed shell fragment) were obtained both with and without the explicit inclusion of water molecules according to the following protocol: (*a*) self-consistent-field (SCF) molecular orbital calculations were performed using the GAUSSIAN 98 suite of programs (110); (*b*) all geometries were fully optimized using conjugate gradient methods (111) without any symmetry constraints initially using Hartree-Fock theory with the 6-31G(d,p) split valence basis set (112); (*c*) the HF/6-31G(d,p) minimum energy conformations were then refined with density functional theory with Becke's 3 parameter functional (B3LYP) (113) with the same basis set; and (*d*) electrostatic potential—derived, atom-centered partial charges were obtained for the B3LYP/6-31G(d,p) minimum energy clusters according to the CHelpG scheme (114).

Paddison et al. began their molecular work (101) by coupling electronic structure calculations with continuum dielectric modeling (115) of trifluoromethane sulfonic (triflic) acid in an effort to secure molecular information concerning the interaction of water with the terminal portion of the side chains of Nafion. In this work, they calculated the relative potential energy as a function of rotation about the sulfur- (hydroxyl) oxygen bond (i.e., CF_3SO_2–OH), displayed in Figure 4, and determined that with inclusion of the electrostatic interaction of the water, the free energy barrier was substantially reduced for rotation of the acid group into the water medium. In addition, they probed the acidity of CF_3SO_3H with a single water molecule and determined a transition state consisting of the ion pair CF_3SO_3- and H_3O+ with an activation energy of 4.7 kcal/mol after inclusion of electrostatic free energy.

Subsequently, Paddison et al. examined several structural aspects of the side chain of Nafion (102–104) on the premise that this would provide important preliminary information for subsequent proton dynamics modeling. On the basis of a full optimization of the side chain fragment CF_3OCF_3 with a single water molecule, they determined that the ether oxygens in the side chain were not hydrophilic. Figure 5 reveals that the water molecule adopts a position relative to the side chain fragment that is clearly not hydrogen bonded to the oxygen with an O–O distance of 3.16 Å. Because of the strong electron withdrawing effect from the two $–CF_3$ groups, the electron density on the ether oxygen is reduced and thus a hydrogen bond does not form with the water molecule. This finding is consistent with the IR

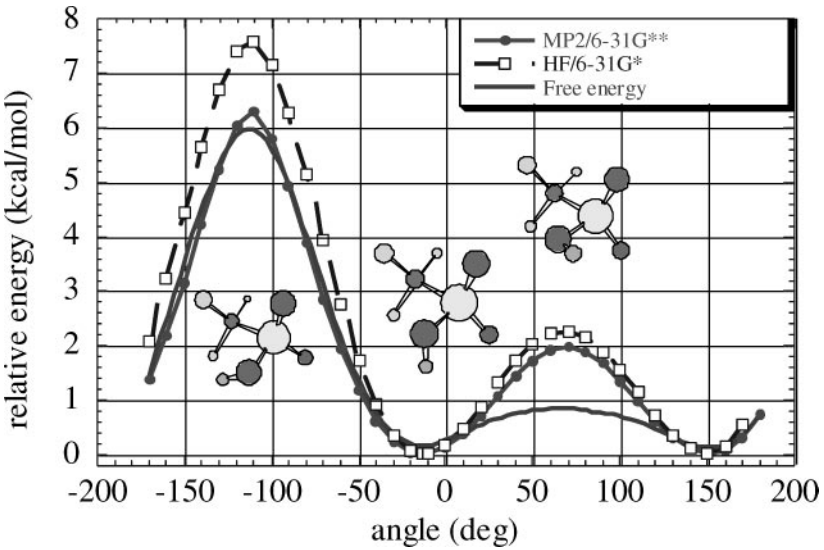

Figure 4 Computed relative potential energy (at the HF/6-31G*, MP2/6-31G**, and corrected MP2/6-31G** for electrostatic solvation free energy according to a continuum dielectric model) as a function of rotation about the sulfur-oxygen bond in triflic acid, i.e., CF_3SO_2–OH. Note the significant reduction in the rotational free energy when the proton is pointed into aqueous/solvent environment. Taken from Reference (101) with permission from Elsevier.

studies of Zanderighi et al. (31) and the molecular dynamics simulations of Vishnyakov & Neimark (116). Full geometry optimizations (at the B3LYP/6-31G** level) of the entire Nafion side chain (103, 104) revealed two distinctly different conformations (Figure 6). These two structures are essentially isoenergetic even though the geometries of the side chains are very different: the conformation in Figure 6*a* is folded, where the two ether oxygens in the chain are *gauche* relative to one another, and the total length of the chain is only 5.0 Å [as measured by the distance from C(1) to H(26)]. The conformation in Figure 6*b* is an elongated or unfolded conformation, where the ether oxygen atoms adopt a *trans* configuration with a corresponding side chain length of 10.0 Å. The potential energy barrier height for the unfolding of the side chain (i.e., from structure 1 to 2) was determined to be about 4.6 kcal/mol from a construction of the potential energy surface (B3LYP/6-31G**) for rotation about the C(6)–C(9) bond, where the electrostatic solvation was accounted for with a continuum dielectric model (115). It is also worth noting that the sulfonic acid group (i.e., $–SO_3H$) adopts a *gauche* conformation relative to the second ether oxygen [i.e., O(15)] in the folded configuration and a *trans* configuration in the elongated conformation. This latter geometry for the side chain was also obtained in the classical molecular dynamics simulations of Vishnyakov & Neimark (117).

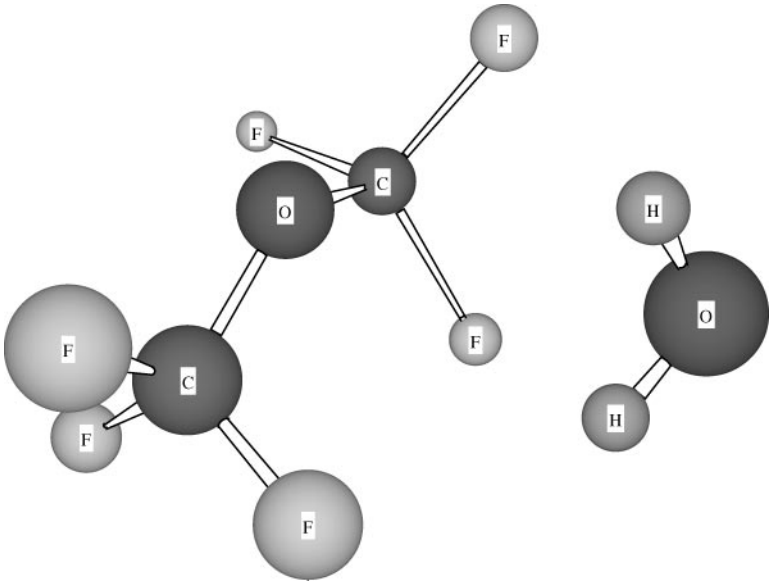

Figure 5 Fully optimized configuration (at the B3LYP/6-31G** level) of di(trifluoromethane) ether with a single probe water molecule. Note that the water molecule does not form a hydrogen bond with the ether oxygen. The O–O distance is >3 Å. Taken from Reference (102) with permission from Elsevier.

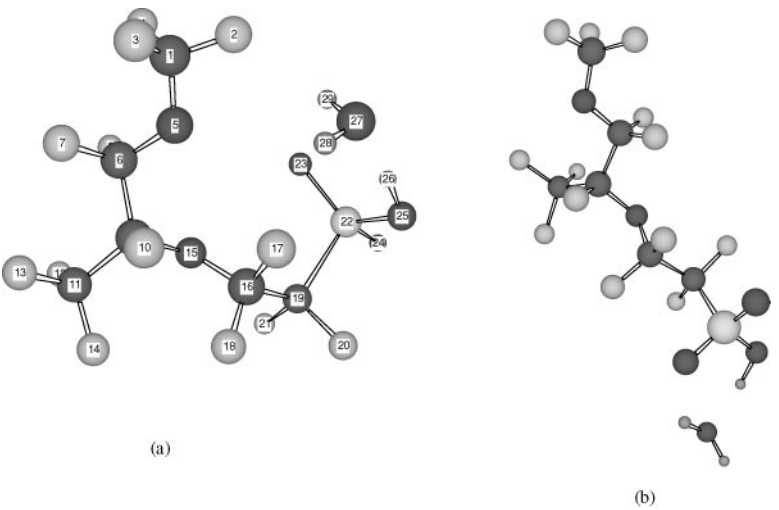

Figure 6 Fully optimized (B3LYP/6-31G**) conformations of the acid side chain of Nafion with a single probe water molecule placed near the terminus of the chain. The conformations are essentially isoenergetic with (*a*) a folded geometry and (*b*) an extended geometry. Taken from Reference (103) with permission from Ecole Polytechnique de Montreal.

In an effort to understand proton dissociation and the stabilization of the dissociated proton in the first hydration shell, Paddison et al. (104–106) conducted a series of explicit water electronic structure calculations with both triflic (as an analog for Nafion) and para-toluene sulfonic (for PEEK) acids. From the optimized geometry of the isolated acid, water molecules were systematically added to the B3LYP/6-31G** minimum energy conformations to obtain successively larger water clusters of the acid (i.e., $–SO_3H + nH_2Os$, $1 \leq n \leq 6$).

No dissociation of the proton was observed with either CF_3SO_3H or $CH_3C_6H_4SO_3H$ until three water molecules were added; the conformations for the sulfonate-hydronium ion pair are displayed in Figure 7. The formation of a hydronium ion is favored through the formation of hydrogen bonds with two water molecules and one of the oxygens of the now formed triflate anion. The dissociated state is adopted as a result of the excess positive charge being stabilized in the hydrogen bonding network, and the excess electron density (due to the breaking of the $–SO_3–H$ bond) being sufficiently delocalized by the neighboring group: $–CF_3$ or $–C_6H_4CH_3$. It is the combination of these two effects that result in a minimum energy conformation for each cluster showing a dissociated proton. The separation of the proton from the resulting anion (as measured by the distance of the oxygen on the hydronium ion to the sulfonate oxygen from which the proton left) is about the mean of that

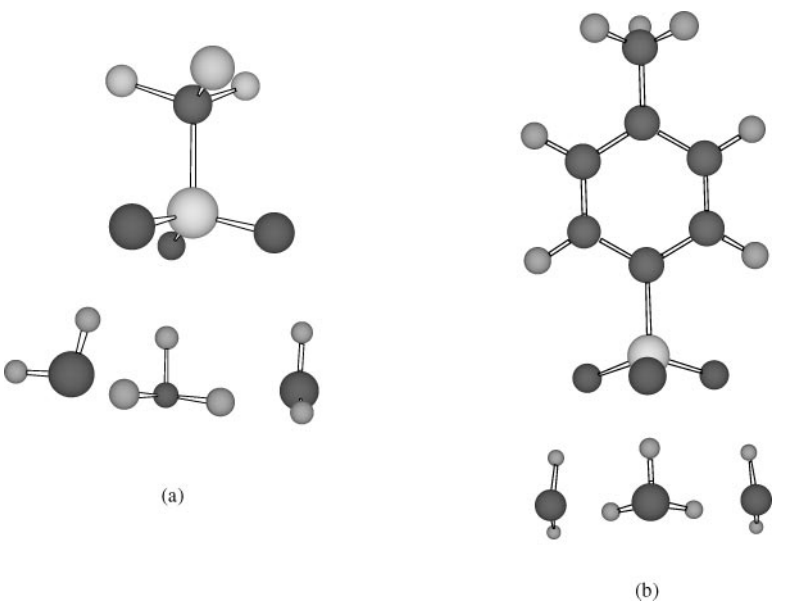

Figure 7 Fully optimized (B3LYP/6-31G**) conformations for clusters with three water molecules showing first dissociation of acidic proton: (*a*) triflic acid and (*b*) para-toluene sulfonic acid. In both cases the dissociated proton forms a hydronium ion, but its equilibrium position is closer to the sulfonate anion for the aromatic system. Taken from Reference (106) with permission from Ecole Polytechnique de Montreal.

observed in the Eigen ($H_9O_4^+$, 2.60 Å) and Zundel ($H_5O_2^+$, 2.50 Å) ions in bulk water (98) for the perfluoro system, but somewhat smaller for the aromatic system (∼2.4 Å). The difference between the two minimum energy conformations is due to the difference in the partial charge residing on the oxygen atoms. The clusters formed with four and five water molecules (106, 108) are similar to those observed with three water molecules in that the hydronium ion forms a contact ion pair with the sulfonate anion. However, the hydronium ion adopts a position progressively farther away from the anion as the number of water molecules in the cluster is increased from three to five.

When a sixth water molecule is added, a complete separation of the excess proton (as a hydronium ion) from the anion takes place. Minimum energy conformations (B3LYP/6-31G**) for triflic and para-toluene sulfonic acids are shown in Figure 8. This result was consistently observed for optimizations begun from a variety of starting geometries. Here, the hydronium ion forms a true Eigen ion as it is hydrogen bonded to three water molecules with an average O–O distance of 2.56 Å. Of additional significance is the observation that the hydronium ion is significantly

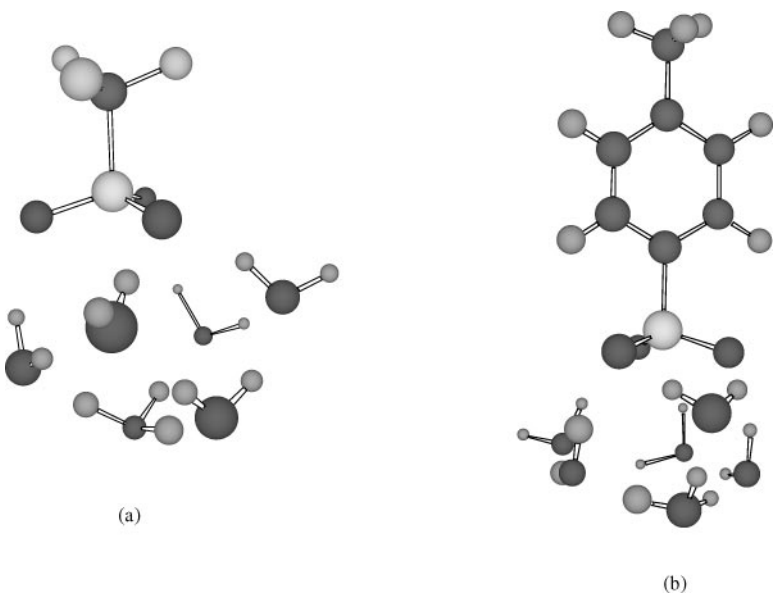

Figure 8 Fully optimized (B3LYP/6-31G**) conformations for clusters with six water molecules showing separation of the hydrated proton from the conjugate anion: (*a*) triflic acid and (*b*) para-toluene sulfonic acid. In both cases the proton forms an Eigen ion (hydrated hydronium ion). The average O–O distance between the oxygen atom of the hydronium ion and the sulfonate oxygen atoms is (*a*) 4.24 Å and (*b*) 3.64 Å, attesting to the stronger Lewis basicity of the aromatic system. Taken from Reference (106) with permission from Ecole Polytechnique de Montreal.

farther away from the anion with the cluster consisting of six water molecules, as was observed in the contact ion pair minimum energy conformations: 4.2 versus 2.6 Å for CF_3SO_3H and 3.6 versus 2.4 Å for $CH_3C_6H_4SO_3H$. The trend in the hydrogen bond length (O–O) witnessed in the smaller water clusters is consistent with that observed after separation of the proton occurs. This suggests that with sufficient water (i.e., with 6 H_2Os) the proton is shielded from direct electrostatic interaction with the sulfonate anion by an intermediate layer of water molecules. These theoretical results are consistent with the interpretation of the IR spectra measured by Zanderighi et al. (31). This also suggests that the first hydration shell of the sulfonate anions in these membranes consists of five water molecules.

All these conformational differences may be rationalized in terms of the differences in the strength of the acids and conjugate bases. Triflic acid is a superacid and substantially stronger (in a Lewis acid sense) than para-toluene sulfonic acid. Upon dissociation of the proton, electron density on the sulfonate anion is delocalized in both systems. However, in the aromatic system it is delocalized in the π-ring, and in the perfluorinated system, it is withdrawn and stabilized by the $-CF_3$ group. The conjugate Lewis base (i.e., the sulfonate anion) that is formed is stronger in the case of the para-toluene sulfonate anion than for the triflate anion. The strength of the conjugate base has a direct bearing on the position of the dissociated proton: The proton will interact more strongly in the case of the stronger conjugate base, i.e., para-toluene sulfonate. A quantitative sense of the relative strength of the conjugate bases (i.e., the sulfonate anions) was determined through calculation of the total atomic charge residing on the sulfonate oxygens atoms. With the ChelpG routine (114), it was observed that the para-toluene sulfonate anion oxygens had substantially more negative charge for all the water clusters (108). The differences in the strength of the conjugate base (sulfonate anion) will affect the hydrogen bonding of the water molecules and the consequent transport of protons. This will be particularly important under conditions of minimal water content.

In a recent investigation, Paddison performed a series of explicit water electronic structure calculations with the side chain of the Dow membrane, i.e., $CF_3OCF_2CF_2SO_3H$ (109). Similar to the triflic and para-toluene sulfonic acids, proton dissociation was observed only after the third water molecule was added. However, with the addition of a fourth water molecule, two equilibrium conformations were observed and are displayed in Figure 9. In the first conformation, the hydronium ion is hydrogen bonded to the sulfonate anion at the termini of the chain similar to the structures observed in the four water clusters with triflic and para-toluene sulfonic acids. However, in the second minimum energy structure, the proton (hydronium ion) is separated from the anion and shielded with the three water molecules in a high-symmetry arrangement that has formed an Eigen ion. The O–O distance in this Eigen ion is 2.55 Å and is only slightly shorter than the O–O distance observed for the Eigen ion in bulk water (2.6 Å; see above). Of significance in comparing these two global, yet distinct, minimum energy structures is that the one exhibiting the separated proton is 2.3 kcal/mol lower in energy. Clearly, the latter structure is the thermodynamically favored conformation.

A final observation worth noting in the water clusters was the substantial increase in the distance of the acidic proton from the CF_3 group on the backbone as the water molecules were added. This distance was observed to increase from 6.2 Å for the isolated chain to 8.9 Å for the cluster with six water molecules. This latter observation is consistent with the earlier work of Paddison et al. (102), where the complete Nafion side chain was observed to be fairly stiff.

Although these electronic structure calculations have provided structural information concerning the hydrophilic portion of the PEMs and, even more importantly, molecular-scale information concerning the dissociation of the proton and hydration of the anionic fixed site, all these calculations were performed on single isolated fragments, and thus the effects of a distribution of sulfonic acid groups or even the role of a neighboring side chain have not been examined. In addition, the above calculations have sought to rationalize fundamental understanding of the mechanisms of proton transfer through examination of only static equilibrium structures. Thus these molecular orbital calculations do not reveal specific information concerning the dynamics of the proton. In the next section, the role of a neighboring sulfonic acid group is examined along with an investigation into proton dynamics in a model system for a minimally hydrated PEM.

The Role of the Side Chain of a PEM in Proton Transfer

It is important to state here that the question of what specific role the side chains play in proton conduction in PEMs has been raised by many, including synthetic polymer chemists, but it is far from completely understood. Unfortunately, there is at present no real insight coming from any experiments other than the observation that the length or presence of a side chain can affect the proton conductivity of the membrane, particularly at low degrees of hydration (118). Recently, Paddison (119) performed a series of first principles electronic structure calculations on a fragment of the Dow PEM consisting of two side chains to attempt a molecular understanding of the potential role of the side chain in the transfer of protons. While the information obtained from this work does not fully answer this question, the results of this work are discussed below.

This series of electronic structure calculations (119) does represent a significant advancement of previous work (101–104, 106, 107) due to the large number of atoms (and electrons) treated at the B3LYP/6-31G** level of theory. Only a few years ago full optimizations on such large electronic systems could not be performed in any practical manner (i.e., in reasonable lengths of time) on all but a few of the largest and fastest computers. As it is, these calculations were performed with eight processors (450 MHz P-III) running in parallel on each job and required several weeks (per job) to obtain the minimum energy conformation from carefully selected starting geometries. The chosen fragment of the Dow membrane consisted of two complete side chains (i.e., $–OCF_2CF_2SO_3H$) and a backbone consisting of eight difluoromethylene (i.e., $–CF_2–$) groups, thus corresponding to a membrane with an equivalent weight of about 750.

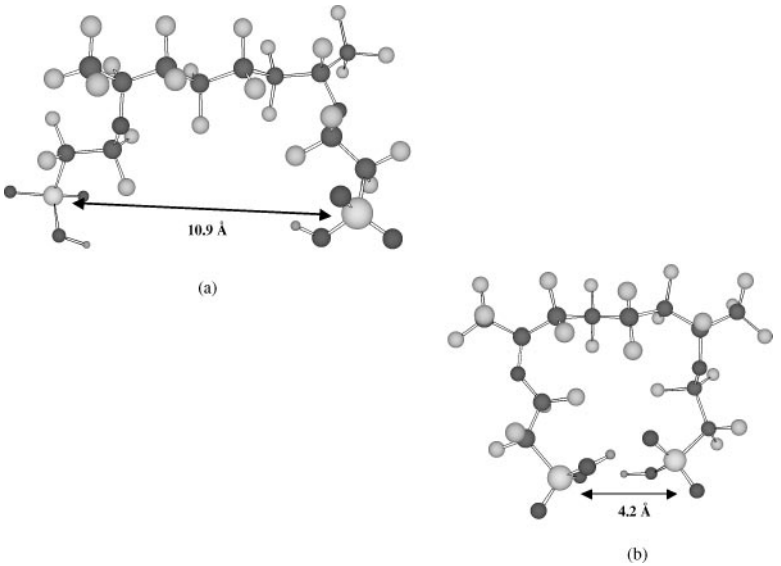

Figure 10 Fully optimized (B3LYP/6-31G**) conformations for a two–side chain fragment of the Dow PEM. These are large electronic systems with 48 atoms. The difference in the two conformations is highlighted with the S-S distance indicated. The conformation in (*b*) is formed by two hydrogen bonds between the sulfonic acid groups and is a significant 12.3 kcal/mol lower in energy than the conformation in (*a*).

Optimizations were performed according to their standard protocol (see above), and for the isolated fragment (i.e., without the addition of any water molecules), two distinctly different minimum energy conformations were obtained. In Figure 10*a* a global minimum for the fragment was obtained with the two side chains well separated from one another with a sulfur-to-sulfur distance of nearly 11 Å. In contrast, Figure 10*b* shows a conformation where the sulfonic acid groups have formed two hydrogen bonds, and thus there is only slightly greater than 4 Å between the termini of the pendant chains. Of significance in comparing the two minimum energy structures is that the structure showing the two side chains interacting is considerably lower in energy (i.e., 12.2 kcal/mol!) and therefore suggests the preference of the side chains to interact even without water present in the polymer. Furthermore, Paddison observed that when three water molecules were added to the conformation in Figure 10*a*, the termini of the side chains came together with a separation of only 6.2 Å. Clearly, the hydrogen bonding of the sulfonic acid groups is favored, and with even minimal water in the membrane, a continuous network of water is likely to be formed among the $–SO_3H$ groups.

With the addition of four water molecules to the Dow membrane fragment, two distinctly different minimum energy conformations were observed. Shown in Figure 11*a* is a conformation where no protons are dissociated from the sulfonic

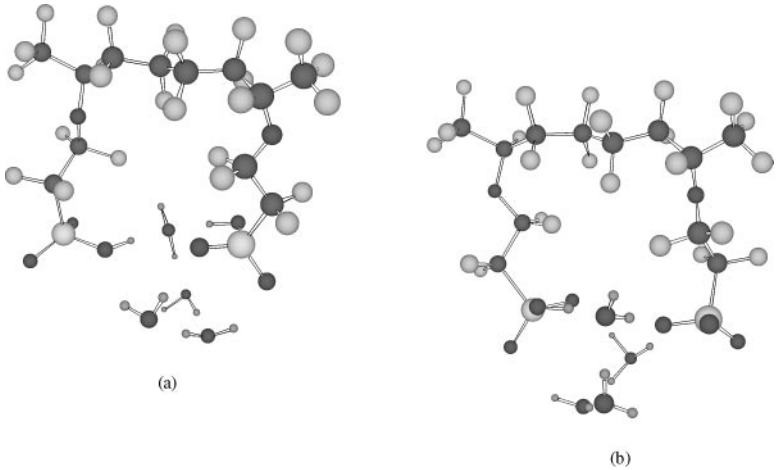

Figure 11 Fully optimized (B3LYP/6-31G**) conformations for the two–side chain fragment of the Dow PEM with four water molecules. The conformation in (*b*) shows dissociation of one of the acidic protons (i.e., the formation of a hydronium ion) and is favored over the conformation in (*a*), where no dissociation of the protons has occurred, with a difference in energy of 5.0 kcal/mol.

acid groups, but where a single water molecule is pinned between the acidic protons. In contrast, Figure 11*b* displays an optimized structure where one proton is dissociated and has formed a hydronium ion that is hydrogen bonded to both side chain termini. Once again there is an appreciable energy difference between the two structures, with the one exhibiting partial (i.e., one of the two acidic protons) dissociation being more favorable by 5.0 kcal/mol. The latter result in this di-sulfonic acid polymer fragment does suggest, in contrast to the single triflic acid water cluster results (104, 109), that it does not require a water content of at least 3 H_2Os/SO_3H for some (i.e., partial) proton dissociation to occur. This refined result is consistent with the IR results of Zanderighi et al. (31).

Finally, Paddison (119) found that to obtain dissociation of both protons, a cluster consisting of six water molecules is required. Figure 12 displays a minimum energy conformation of the Dow membrane fragment with six water molecules, where one of the dissociated protons has formed a hydronium ion that is hydrogen bonded to both sulfonate anions and the other proton has formed a Zundel ion. Of several fully optimized structures of the fragment with six water molecules, the one with the dissociation of both protons was the lowest in energy. Attempts to locate a minimum energy structure with the delocalized proton bonded to either of the water molecules in the Zundel ion always resulted in a structure similar to the one displayed in Figure 12. This result is most interesting, as it represents one (see below) of the first reported electronic structure results with a Zundel ion present in a minimum energy conformation. As was discussed above, the Zundel

ion plays an important role in the diffusion of protons in bulk water, which indicates that this ion is essential in the transfer/transport of protons in PEMs of minimal hydration. Additional theoretical evidence for the role of the Zundel ion is reported in the proton dynamics work described below.

Proton Dynamics in a Model PEM

One of the short comings in all of the electronic structure calculations discussed thus far (101–109, 119) is the fact that these calculations seek to understand structure and mechanism through static minimum energy conformations and therefore do not address the dynamics of any of these systems. With this in mind, recently Paddison et al. (120, 121) carried out groundbreaking ab initio molecular dynamics simulations of the model system trifluoromethane sulfonic acid monohydrate solid $(CF_3SO_3^- H_3O^+)_4$ (for a minimally hydrated Nafion PEM). This solid is a reference system with a well-defined crystallographic structure (122), with a low hydration level of one water molecule per sulfonate head group, and for which controlled molecular dynamics simulations are feasible. A transition was observed from the stable (i.e., native solid) state with localized protons (as hydronium ions) to a defect state with two delocalized protons. These two states for the solid are shown in Figure 13. One of these protons nucleates a Zundel ion ($H_5O_2^+$), whereas the other one is accommodated between the oxygens of two sulfonate groups. The formation of the latter sulfonate O•••H•••O complex required a considerable rearrangement of the crystal structure so that the oxygens could approach each other at hydrogen bond distance. As described above, the Zundel ion is known to be important in the

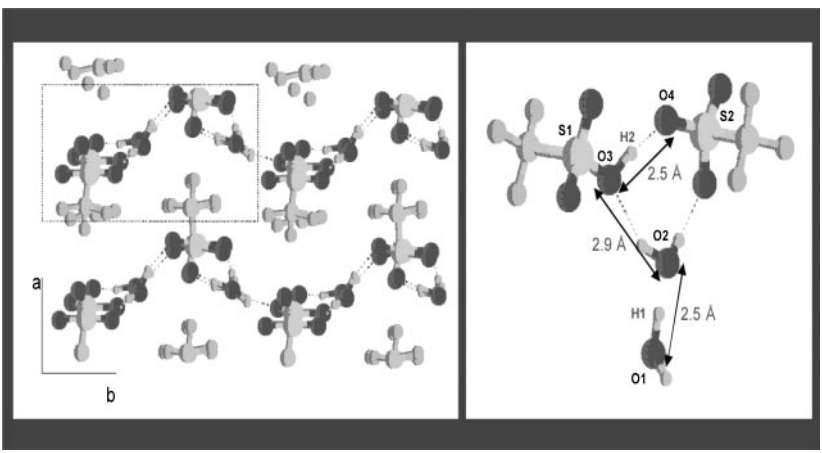

Figure 13 Snapshots from ab initio molecular dynamics simulations of the trifluoromethane sulfonic acid monohydrate solid. Picture on the left is the native solid and the picture on the right is the stable defect structure showing the two delocalized protons; one shared by the sulfonate anions and the other as a Zundel ion.

diffusion of protons in bulk water (96–100). This work along with that described above, however, are the first characterizations of its role in systems with minimal water. These two proton-stabilized structures interact to lower the energy of the intermediate state.

The free energy of formation of the defect state was calculated to be 0.25 eV from a quasiharmonic model based upon statistical determination of normal models (121) and is displayed in Figure 14. This energy difference corresponds

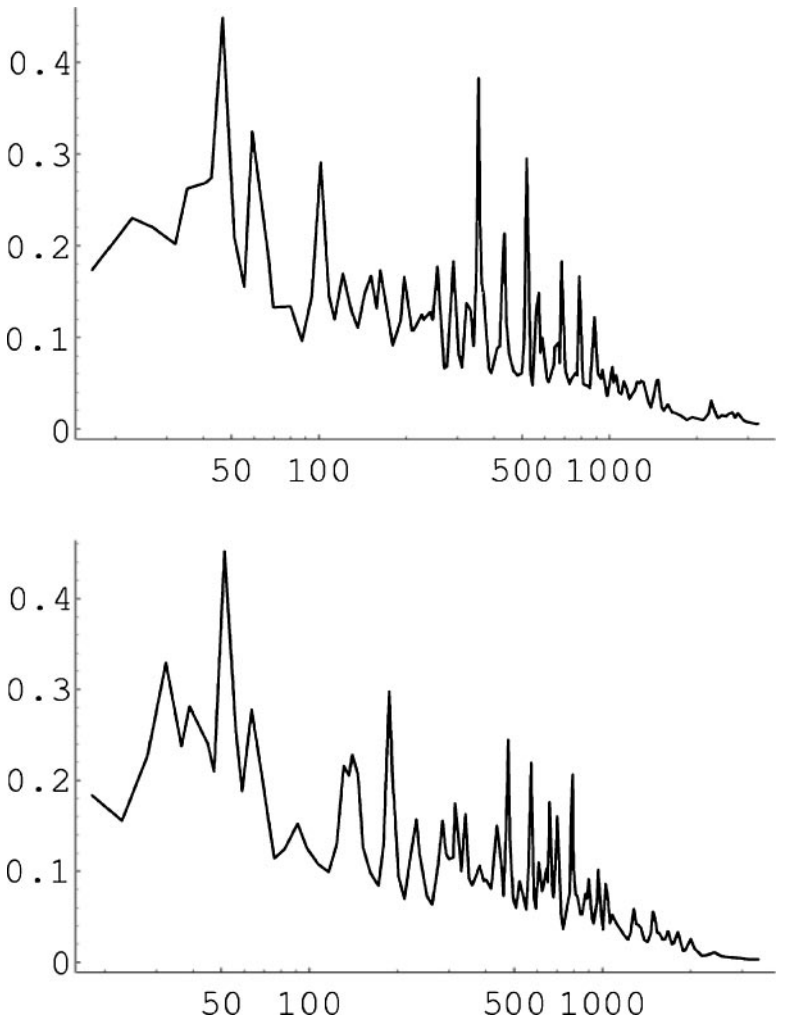

Figure 14 Spectral density of vibrational states for the native solid (*upper*) and stable defect of trifluoromethane sulfonic acid solid (*lower*) plotted as a function of wavenumber (cm^{-1}). Notice the enhancement of nodes in the defect state around 50 cm^{-1}, which attests to the presence of the delocalized protons.

well with experimental measurement of the activation energy for proton transport in minimally hydrated Nafion (123). The plot of the spectral density in the defect state shows the expected increase in soft modes associated with the presence of the delocalized protons. An observed drift of the Zundel ion indicates its function as a mediator of proton transfer, working as a relay site between hydronium ions or sulfonate anions. The observations of the concerted dynamics in the solid indicate that an appropriate flexibility of anionic side chains is an important ingredient of proton transport in PEMs under conditions of minimal water content and high anion concentrations. This latter result is consistent with the electronic structure results discussed earlier (103, 119).

The theoretical work described thus far has sought to provide a fundamental underpinning to the mechanisms of proton conduction in partially hydrated PEMs through an examination of chemical structure, hydration, proton dissociation, and proton transfer to the water domain, with first principles methods. This is very important information and most of what has been presented agrees well in a qualitative sense to known experimental observations of these materials. What is lacking in this work is a direct connection to quantitative experimentally measurable parameters. Efforts that have attempted to model proton transport and diffusion processes are discussed below.

Proton Transport and Diffusion in the Water of PEMs

A number of physical and theoretical models have been developed in an effort to elucidate water and ion transport in ionomer membranes. Most of these models differ markedly from the theoretical work described in the previous sections, as a certain amount of coarse-graining in the form of phenomenological parameters and ideas have been introduced.

In the early work of Breslau & Miller (124), a hydrodynamic approach was used to model electroosmosis in ion-exchange membranes. The ions were treated as macroscopic spheres in a homogeneous medium, with the membrane modeled as either a cylindrical or a parallel plate pore. Their model was able to predict electroosmotic drag coefficients within 5% of experimental values, with the important exception of the proton where the agreement was poor. Starting from the assumptions and model of Gierke et al. (24, 67, 68), Capeci et al. (125) constructed salt solubility and anion transport models based on phenomenological equations and showed that the narrow pores dominate ion and solvent transport in the membrane. Verbrugge & Hill (126) developed a macro-homogeneous model (the membrane and pore fluid were considered as one phase, and ion fluxes and solvent transport related without specifying a molecular-level mechanism) to describe both ion and solvent transport with the Stefan-Maxwell equations, including transport by diffusion, migration, and convection. Pintauro & Verbrugge (127) developed a partition coefficient model for an arbitrary electrolyte-filled pore. They attempted to simulate specific adsorption of pore-electrolyte species onto the pore-surface fixed-charge sites, effects of hydration, and dipole alignment of the electrolyte to an electric field. Their model was extended by Bontha & Pintauro (128) to

the specific treatment of Nafion: modeling the membrane as an array of parallel cylindrical pores and incorporating electrostatic interactions between wall charges and mobile counterions and coions, with solvent dipole alignment due to the wall charges (fixed) and counterion and coion hydration–free energy changes occurring as the ions are solvated in the pore fluid.

From a slightly different perspective, Eikerling et al. (129) developed a phenomenological random network model of a microporous PEM with an effective medium. They assumed a hydrated morphology for the PEM similar to the proposed model of Gierke et al. (24, 67, 68) and were able to demonstrate the importance of the connectivity of the pores and the coordination of the water in the pores to the overall conductivity of the membrane. Furthermore, from the results of their simulations, they concluded that PEMs with more elastic properties (as opposed to softer PEMs) would swell more homogeneously, resulting in good connectivity of the pores and consequently higher conductivity. More recently, Eikerling et al. derived another phenomenological model (130) where the mobility of the protons is assumed to occur via two mechanisms: a surface mechanism where proton transport proceeds along the array of acid groups (i.e., via structure diffusion) over the interface, and a bulk mechanism where the protons are transported with the Grotthuss mechanism. A single pore (with an assumed plane geometry) model (131) was used to show that the activation energy of the surface mechanism contributes considerably to the work terms owing to interactions of the protons with the fixed sites and consequent low mobility. This model also revealed that these work terms vanish in the central region of the pore, resulting in bulk-like proton mobility with low activation energy. However, their model was based on the assumption that the concentration of protons is greatest at the surface of the pore. This is in contrast to the FTIR study of hydrated cast Nafion films by Zanderighi (31) and Brownian dynamics simulations of cylindrical nanopores (132).

Din & Michaelides (133) reported molecular dynamics simulations of micropores (9.36 and 12.24 Å in diameter) swollen with water and protons possessing uniform charge density on the walls. They concluded that the classic Poisson-Boltzmann theory did not correctly predict the distribution of protons within the pores and were unable to correctly determine electroosmotic drag coefficients in Nafion, attributing this to the simplicity of their description of charge distribution on the walls of the pores.

A significant contribution toward the development of a proton and water transport model for hydrated PEMs has recently been developed by Paddison et al. (134–140). They use a nonequilibrium statistical mechanical framework to compute the self-diffusion coefficient of a proton in an arbitrary membrane pore/channel. Their model has demonstrated remarkable predictive capability for Nafion and PEEKK membranes over a range of water contents. A complete derivation of the model can be found in References 135, 136. The remainder of this section discusses some of the relevant highlights of their work. Their model seeks to connect the molecular structure and hydrated morphology of an arbitrary PEM with the measurable and macroscopic quantity of the proton self-diffusion coefficient. Factors affecting

the coupled transport of a proton and a water molecule (i.e., a hydronium ion, designated subscript α in the model equations below) are examined in a hydrated pore/channel of a PEM ex situ of a fuel cell configuration. The Einstein relation

$$D_\alpha = \frac{kT}{\zeta_\alpha} \tag{3.}$$

establishes the inverse relationship of the diffusion coefficient with the friction coefficient. While the Stokes relation ($\zeta = 6\pi\eta a$) is commonly used to compute friction coefficients for macroscopic objects moving in viscous media (and with Equation 3 forms the Stokes-Einstein formula), in their model the methods of nonequilibrium statistical mechanics are used to compute the average force experienced by a hydronium ion moving in the pore, making use of the fundamental definition of the friction coefficient

$$\langle \mathbf{F}_\alpha \rangle = -\underline{\underline{\zeta}} \cdot \mathbf{v}_\alpha, \tag{4.}$$

where $\mathbf{v}_\alpha$ is the velocity (assumed to be constant) of the hydronium ion. Thus from these two equations, the diffusion coefficient is evaluated from a computation of the average force.

The pore of the PEM is assumed to possess a cylindrical geometry with length L and cross-sectional radius R, filled with N water molecules, each possessing a dipole moment μ. The dissociated sulfonic acid functional groups ($-SO_3^-$) in the pore are modeled as n radially symmetric axially periodic arrays of fixed ions (i.e., point charges), each possessing a charge of $-e$. The average force experienced by the hydronium ion is calculated from the standard relation (from statistical mechanics):

$$\langle \mathbf{F}_\alpha \rangle (\mathbf{r}_\alpha) = \int d\mathbf{r}\, d\mathbf{p} \mathbf{F}_\alpha(\mathbf{r}_\alpha, \mathbf{r}) \rho(\mathbf{r}_\alpha, \mathbf{p}, \mathbf{r}), \tag{5.}$$

where $\mathbf{r}_\alpha$ denotes the position of the hydronium ion. The average (integration) is over the position, $\mathbf{r}$, and conjugate momentum, $\mathbf{p}$, of all the N water molecules, of the net force on the hydronium weighted with a phase space distribution function $\rho(\mathbf{r}_\alpha, \mathbf{p}, \mathbf{r})$. This distribution function is obtained from the more general time-dependent distribution function, a solution of the time evolution or Liouville equation:

$$i \frac{\partial \rho(\mathbf{r}_\alpha, \mathbf{p}, \mathbf{r}, t)}{\partial t} = L_0 \rho(\mathbf{r}_\alpha, \mathbf{p}, \mathbf{r}, t), \tag{6.}$$

where L_0 is the Liouville operator for the system with a coordinate reference system moving with constant velocity $\mathbf{v}_\alpha$. The Liouville operator is defined by the Poisson bracket:

$$L_0 = i \{H_0(\mathbf{r}_\alpha, \mathbf{p}, \mathbf{r})\}, \tag{7.}$$

where $H_0(\mathbf{r}_\alpha, \mathbf{p}, \mathbf{r})$ is the Hamiltonian for the pore. The total energy of the pore consists of the kinetic energy of all the water molecules and the net potential energy, $V(\mathbf{r}_\alpha, \mathbf{r})$, due to two-body interactions of the water molecules, hydronium ion,

and fixed sites according to

$$H_0(\mathbf{r}_\alpha, \mathbf{p}, \mathbf{r}) = \sum_{i=1}^{N} \frac{m(\mathbf{v}_i + \mathbf{v}_\alpha)^2}{2} + V(\mathbf{r}_\alpha, \mathbf{r}), \tag{8.}$$

where m is the mass and $\mathbf{v}_i$ the velocity of the i^{th} water molecule. The latter term in Equation 8 consists of the following four terms:

$$V(\mathbf{r}_\alpha, \mathbf{r}) = -\sum_{i=1}^{N} \frac{\mu^2 e^2}{48\pi^2 \varepsilon^2 kT} \frac{1}{|\mathbf{r}_\alpha - \mathbf{r}_i|^4} + \Psi_0 \cos\left(\frac{2\pi n z_\alpha}{L}\right) + \sum_{i<j}^{N} \frac{2\mu^4}{3(4\pi\varepsilon)^2 kT} \frac{1}{|\mathbf{r}_i - \mathbf{r}_j|^6} - \sum_{i=1}^{N} \frac{2\pi\mu\Psi_0 n}{eL} \sin\left(\frac{2\pi n z_i}{L}\right), \tag{9.}$$

where ε is the permittivity of the water in the pore, k the Boltzmann constant, T the temperature, and Ψ_0 the amplitude of the potential energy owing to interaction of the hydronium ion with the $-SO_3^-$ groups. These respective contributions to the potential energy of the system are due to (*a*) interactions of the hydronium ion with the water molecules, (*b*) interaction of the hydronium ion with the arrays of the fixed sites, (*c*) water-water interactions, and (*d*) interactions of the water molecules with the fixed sites. A formal solution of Equation 6 is

$$\rho(\mathbf{r}_\alpha, \mathbf{p}, \mathbf{r}, t) = e^{-iL_0 t}\rho(\mathbf{r}_\alpha, \mathbf{p}, \mathbf{r}, 0) = e^{-iL_0 t}\rho_{eq}(\mathbf{r}_\alpha, \mathbf{p}, \mathbf{r}), \tag{10.}$$

where $\rho_{eq}(\mathbf{r}_\alpha, \mathbf{p}, \mathbf{r})$ is the distribution function under equilibrium conditions. A nonequilibrium stationary state (moving with the ion), described by the distribution function in Equation 5, is obtained in the limit of $t \to \infty$ in Equation 10. The total force required in Equation 5 is determined by taking the action of the Liouville operator on the momentum of the hydronium ion. Combining these results, one obtains an expression for the scalar friction coefficient of the hydronium that consists of four force-force correlation functions:

$$\zeta_\alpha = \frac{\beta}{3}\int_0^\infty dt\left(\left\langle \mathbf{F}_{\alpha s} e^{-iL_0 t}\mathbf{F}_{\alpha s}\right\rangle_0 + \left\langle \mathbf{F}_{\alpha s} e^{-iL_0 t}\mathbf{F}_{ps}\right\rangle_0 + \left\langle \mathbf{F}_{\alpha p} e^{-iL_0 t}\mathbf{F}_{ps}\right\rangle_0 + \left\langle \mathbf{F}_{\alpha p} e^{-iL_0 t}\mathbf{F}_{\alpha s}\right\rangle_0\right), \tag{11.}$$

where $\beta = 1/kT$, and the forces $\mathbf{F}_{\alpha s}$, $\mathbf{F}_{ps}$, and $\mathbf{F}_{\alpha p}$ are between the hydronium ion and the water molecules, the fixed sites and the water molecules, and the hydronium ion and the fixed sites, respectively. Only the latter three terms in Equation 11 are explicitly evaluated; their sum is taken to be a correction, $\zeta^{(c)}$, to the friction coefficient of the proton in water, i.e.,

$$\zeta^{(c)} = \zeta_2 + \zeta_3 + \zeta_4. \tag{12.}$$

The first force-force correlation function, ζ_1, involves only the force the water exerts on the hydronium ion ($\mathbf{F}_{\alpha s}$) and thus is taken to be either the friction coefficient of a hydronium ion in bulk water calculated with the Stokes relation or the friction coefficient of a proton in bulk water derived from experimental

diffusion measurements. The choice of the numerical value of ζ_1 is not arbitrary but is dependent on the characteristics or nature of the water in the pore, the latter of which is assessed using the dielectric saturation model of Paul & Paddison (84–86).

Thus with this transport model, friction coefficients are computed for a proton (as a hydronium ion) moving in a PEM pore and with the Einstein relation (i.e., Equation 3), the self diffusion coefficient, calculated. The model contains no adjustable or phenomenological parameters but requires basic hydrated morphology information including the dimensions of the pores, degree of hydration, and distribution of anionic (i.e., sulfonate) fixed sites. These parameters are taken from information obtained from ab initio modeling (as presented above) and SAXS experiments (6, 76).

With their model, Paddison et al. (137–140) computed proton diffusion coefficients for Nafion 117 and 65% sulfonated PEEKK membranes at hydration levels where the number of water molecules per sulfonic acid fixed site were 6, 13, and 22.5, and 15, 23, and 30, respectively. The computed coefficients along with the corresponding experimental values obtained from pulsed-field gradient NMR measurements (6, 76) are plotted in Figure 15. The agreement with pulsed-field gradient NMR diffusion measurements is remarkable for both membranes across the entire range of membrane hydration, with the computed values all slightly (<15% difference) lower than experimental ones. As the diffusion coefficients

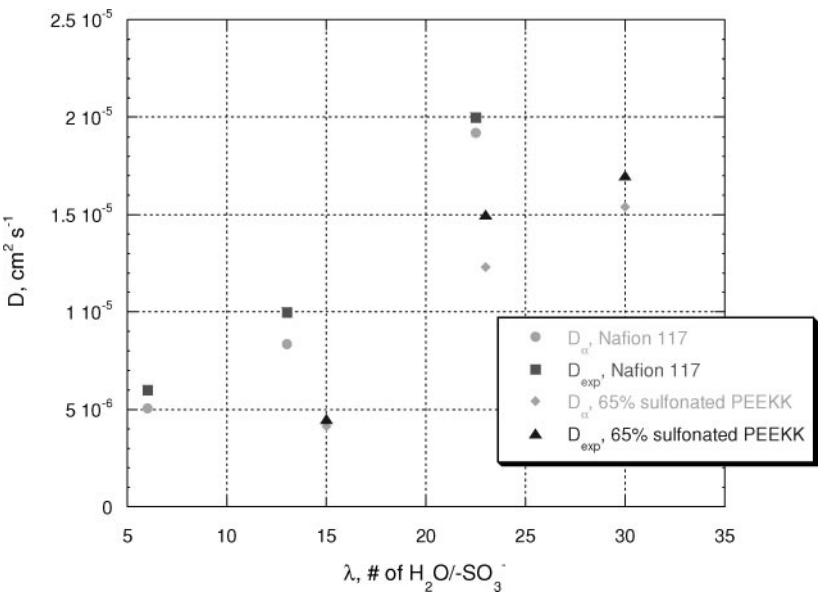

Figure 15 Computed and experimentally determined proton self-diffusion coefficients in Nafion 117 and 65% sulfonated PEEKK membranes as a function of water content. Note the excellent agreement (within 15%) between the calculated and measured values across the range of membrane hydration. Taken from Reference (106) with permission from Ecole Polytechnique de Montreal.

vary over nearly an order of magnitude, this work demonstrates the substantial predictive capability of their transport model, particularly when one is aware that there are no fitting or adjustable parameters in the model.

In a separate investigation, Paddison et al. (136) determined the sensitivity of their transport model to various input parameters, including pore dimensions and distribution of fixed sites. In a particularly insightful case study, they calculated friction and diffusion coefficients for a PEM pore with fixed dimensions ($R = 8$ and $L = 30$), constant hydration level (6 H_2Os/SO_3^-), and fixed number of SO_3H groups, but varied both the intrusion and the uniformity of the axial distribution of the fixed sites independently. The results for the proton diffusion coefficient are plotted as a function of the length of the side chain (i.e., intrusion as measured from the pore wall) for various distributions of the fixed sites in Figure 16.

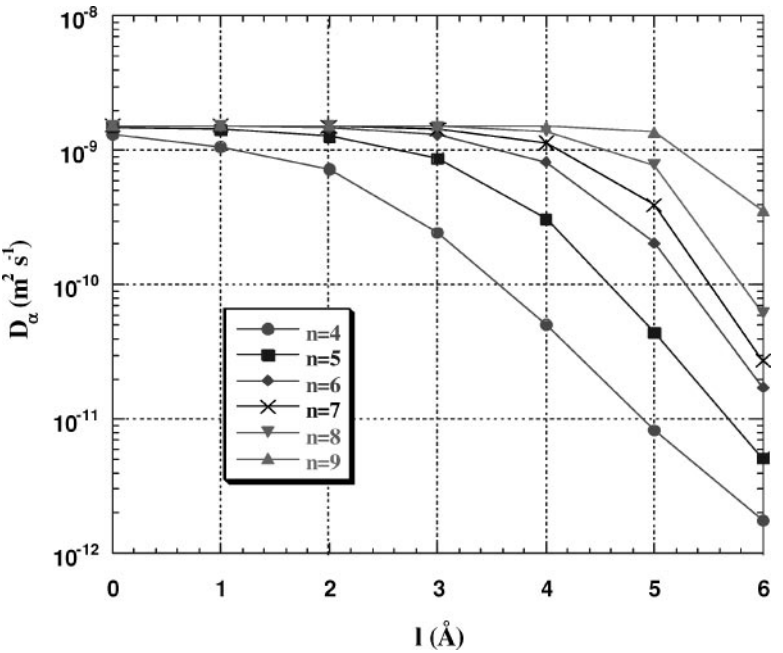

Figure 16 Computed proton diffusion coefficients as a function of the length of intrusion of the side chain (l) and as a function of the number (n) of axially positioned arrays of fixed sites for an arbitrary membrane pore with fixed length, diameter, total number of anionic groups, and water content. Note the substantial sensitivity (i.e., varying over more than three orders of magnitude) of the computed diffusion coefficient to these parameters. The pore with the most uniform distribution of anionic groups (i.e., where $n = 9$) shows the smallest, in fact very little, decrease in the proton diffusion coefficient as the length of protrusion of the anionic groups is increased. Taken from Reference (136) with permission from the American Institute of Physics.

Examination of the plot unequivocally shows the substantial sensitivity of the diffusion coefficient to the intrusion of the sulfonate groups, whereas for a distribution of the sulfonate groups on only four axial arrays (the most heterogeneous distribution examined), the diffusion coefficient varies over four orders of magnitude! In contrast, when the sulfonate groups are distributed uniformly across the length of the pore (i.e., for $n = 9$), the diffusion of the proton is hardly affected by the electric field because of the anionic charges. Thus at minimal water contents, both the intrusion of the side chains and the uniformity of the distribution of the anionic groups have a substantial impact on the proton diffusion in a PEM.

CONCLUSIONS

Although a complete understanding is still forthcoming, this article primarily focuses on a review of the substantial theoretical modeling effort conducted over the past six years that has provided a fundamental molecular-based footing for the mechanisms of proton conduction in PEMs. Specifically, the hydrated morphology, nature of the water in the membrane, and the hydration of the acidic sites have been discussed in the roles they play in the conduction process. Because there are similarities in the diffusion of protons in bulk water to the present topic, an overview of what is understood in bulk water has been provided.

The proton conduction mechanisms in hydrated PEMs may be understood from a consideration of dissociation of the proton from the acidic site, subsequent transfer of the proton to the aqueous medium, screening by water of the hydrated proton from the conjugate base (e.g., the sulfonate anion), and finally diffusion of the proton in the confined water within the polymer matrix. High-frequency dielectric spectroscopy (36, 37) and modeling of the dielectric saturation (84–86) reveal that the confinement of the water in nanodimensioned domains with a strong electrostatic field due to dissociated sulfonic acid groups results in a lower (than in bulk water) permittivity of the water (i.e., water molecules that are more tightly bound to each other and to the fixed sulfonate groups) that inhibits the structural diffusion of the protons, as witnessed in bulk water.

Ab initio electronic structure calculations of polymeric fragments with water (101–109, 119) and quantum molecular dynamics studies on model PEM systems (120, 121) have provided a basis for understanding the molecular ingredients in the conduction process. Specifically, it was determined that (*a*) the dissociated state is adopted as a result of the excess positive charge being stabilized in the hydrogen bonding network of the water molecules, and the excess electron density (due to the breaking of the $–SO_3–H$ bond) sufficiently delocalized by the neighboring chemical group (anchimeric assistance). (*b*) The neighboring chemical group to the sulfonic acid will also impact the preferred separation of the hydronium ion after completion of the first hydration shell. (*c*) Hydrogen bonding between the sulfonic acid groups is favored, and with even minimal water in the membrane there is likely to be a continuous network of water formed among the $–SO_3H$ groups.

(*d*) Partial dissociation of the protons in a PEM will occur at water contents of less than 3 H_2Os/SO_3H. (*e*) The Zundel ion (H_5O_2+) features importantly in the transfer of protons in PEMs of minimal hydration, as it does in bulk water.

The modeling of the transport of protons through single PEM pores with a nonequilibrium statistical mechanical framework (134–140) has provided a remarkably predictive tool for the calculation of the proton self-diffusion coefficient for membranes with distinct morphology, water content, and anionic fixed site distributions. Furthermore, this model has revealed that both the intrusion and the uniformity of the distribution of the anionic groups have a substantial impact on the proton diffusion in PEMs under minimal hydration conditions.

The *Annual Review of Materials Research* is online at http://matsci.annualreviews.org

LITERATURE CITED

1. Steele BCH, Heinzel A. 2001. *Nature* 414: 345–52
2. Savadogo O. 1998. *J. New Mater. Electrochem. Syst.* 1:47–60
3. Sumner JJ, Creager SE, Ma JJ, DesMarteau DD. 1998. *J. Electrochem. Soc.* 145:107–10
4. Creager SE, Sumner JJ, Bailey RD, Ma JJ, Pennington WT, DesMarteau DD. 1999. *Electrochem. Solid State Lett.* 2:434–36
5. Kreuer KD. 1997. *Solid State Ionics* 97:1–15
6. Kreuer KD. 2001. *J. Membr. Sci.* 185:29–39
7. Alberti G, Casciola M, Massinelli L, Bauer B. 2001. *J. Membr. Sci.* 185:73–81
8. Zoppi RA, Yoshida IVP, Nunes SP. 1998. *Polymer* 39:1309–15
9. Aricò AS, Cretí P, Antonucci PC, Antonucci V. 1998. *Electrochem. Solid State Lett.* 1:66–68
10. Bonnet B, Jones DJ, Rozière J, Tchicaya L, Alberti G, et al. 2000. *J. New Mater. Electrochem. Syst.* 3:87–92
11. Kerres J, Ullrich A, Meier F, Häring T. 1999. *Solid State Ionics* 125:243–49
12. Zhang W, Dai G, Kerres J, 1998. *Acta Polym. Sinter.* 5:608–11
13. Lassègues JC. 1992. In *Proton Conductors: Solids, Membranes and Gels-Materials and Devices*, ed. P Colomban, pp. 311–28. Cambridge, MA: Cambridge Univ. Press
14. Wainright JS, Wang JT, Weng D, Savinell RF, Litt M. 1995. *J. Electrochem. Soc.* 142:L121–23
15. Dippel T, Kreuer KD, Lassègues JC, Rodriguez D. 1993. *Solid State Ionics* 61:41–46
16. Bozkurt A, Ise M, Kreuer KD, Meyer WH, Wegner G. 1999. *Solid State Ionics* 125:225–33
17. Wang JT, Wasmus S, Savinell RF. 1996. *J. Electrochem. Soc.* 143:1233–39
18. Yeo SC, Eisenberg A. 1977. *J. Appl. Polym. Sci.* 21:875–98
19. Halim J, Büchi FN, Haas O, Stamm M, Scherer GG. 1994. *Electrochim. Acta* 39:1303–7
20. Gebel G, Lambard J. 1997. *Macromolecules* 30:7914–20
21. Gebel G, Moore RB. 2000. *Macromolecules* 33:4850–55
22. Rollet A-L, Diat O, Gebel G. 2002. *J. Phys. Chem. B* 106:3033–36
23. Rubatat L, Rollet A-L, Gebel G, Diat O. 2002. *Macromolecules* 35:4050–55
24. Gierke TD, Munn GE, Wilson FC. 1981. *J. Polym. Sci. Polym. Phys. Ed.* 19:1687–704

25. Halim J, Scherer GG, Stamm M. 1994. *Macromol. Chem. Phys.* 195:3783–88
26. Roche EJ, Pinéri M, Duplessix R. 1982. *J. Polym. Sci. Polym. Phys. Ed.* 20:107–16
27. Loppinet B, Gebel G, Williams CE. 1997. *J. Phys. Chem. B* 101:1884–92
28. Starkweather HW Jr. 1982. *Macromolecules* 15:320–23
29. Starkweather HW Jr, Chang JJ. 1982. *Macromolecules* 15:752–56
30. Uosaki K, Okazaki K, Kita H. 1990. *J. Electroanal. Chem.* 287:163–69
31. Laporta M, Pegoraro M, Zanderighi L. 1999. *Phys. Chem. Chem. Phys.* 1:4619–28
32. Mauritz KA, Fu R-M. 1988. *Macromolecules* 21:1324–33
33. Mauritz KA, Yun H. 1988. *Macromolecules* 21:2738–43
34. Mauritz KA, Yun H. 1989. *Macromolecules* 22:220–25
35. Chen RS, Jayakody JP, Greenbaum SG, Pak YS, Xu G, et al. 1993. *J. Electrochem. Soc.* 140:889–95
36. Paddison SJ, Reagor DW, Zawodzinski TA Jr. 1998. *J. Electroanal. Chem.* 459: 91–97
37. Paddison SJ, Bender G, Kreuer KD, Nicoloso N, Zawodzinski TA Jr. 2000. *J. New Mater. Electrochem. Syst.* 3:291–300
38. Ceynowa J. 1978. *Polymer* 19:73–76
39. Xue T, Trent JS, Osseo-Asare K. 1989. *J. Membr. Sci.* 45:261–71
40. Rieberer S, Norian KH. 1992. *Ultramicroscopy* 41:225–33
41. Zoppi RA, Yoshida IVP, Nunes SP. 1998. *Polymer* 39:1309–15
42. Lehmani A, Durand-Vidal S, Turq P. 1998. *J. Appl. Polym. Sci.* 68:503–8
43. James PJ, Elliott JA, McMaster TJ, Newton JM, Elliott MS, et al. 2000. *J. Mater. Sci.* 35:5111–19
44. McLean RS, Doyle M, Sauer BB. 2000. *Macromolecules* 33:6541–50
45. Bath BD, Lee RD, White HS, Scott ER. 1998. *Anal. Chem.* 70:1047–58
46. Komoroski RA, Mauritz KA. 1978. *J. Am. Chem. Soc.* 100:7487–89
47. Bunce NJ, Sondheimer SJ, Fyfe CA. 1986. *Macromolecules* 19:333–39
48. Schlick S, Gebel G, Pinéri M, Volino F. 1991. *Macromolecules* 24:3517–21
49. Zawodzinski Jr. TA, Neeman M, Sillerud LO, Gottesfeld S. 1991. *J. Phys. Chem.* 95:6040–44
50. Rankothge HM, Hook J, van Gorkum L, Moran G. 1994. *Magn. Reson. Chem.* 32:446–51
51. Fontanella JJ, Edmondson CA, Wintergill MC, Wu Y, Greenbaum SG. 1996. *Macromolecules* 29:4944–51
52. MacMillan B, Sharp AR, Armstrong RL. 1999. *Polymer* 40:2471–80
53. Alonso-Amigo MG, Schlick S. 1986. *J. Phys. Chem.* 90:6353–58
54. Alonso-Amigo MG, Schlick S. 1989. *Macromolecules* 22:2628–34, 2634–41
55. Heitner-Wirguin C. 1979. *Polymer* 20: 371–74
56. Falk M. 1980. *Can. J. Chem.* 58:1495–501
57. Ostrovskii DI, Brodin AM, Torell LM. 1996. *Solid State Ionics* 85:323–27
58. Heitner-Wirguin C, Bauminger ER, Labensky de Kanter F, Ofer S. 1980. *Polymer* 21:1327–29
59. Rodmacq B, Coey JMD, Pinéri M. 1982. In *Perfluorinated Ionomer Membranes*, ed. A Eisenberg, HL Yeager, pp. 171–94. Washington, DC: Am. Chem. Soc.
60. Martin CR, Rubinstein I, Bard AJ. 1982. *J. Am. Chem. Soc.* 104:4817–24
61. Lee PC, Meisel D. 1980. *J. Am. Chem. Soc.* 102:5477–81
62. Szentirmay MN, Prieto NE, Martin CR. 1985. *J. Phys. Chem.* 89:3017–23
63. Robertson MAF, Yeager HL. 1996. *Macromolecules* 29:5166–71
64. Gavach C, Pamboutzoglou P, Nedyalkov M, Pourcelly G. 1989. *J. Membr. Sci.* 45:37–53
65. Cahan BD, Wainwright JS. 1993. *J. Electrochem. Soc.* 140:L185–86
66. Hashimoto T, Fujimura M, Kawai H. 1982. In *Perfluorinated Ionomer Membranes*, ed. A Eisenberg, HL Yeager,

pp. 217–48. Washington, DC: Am. Chem. Soc.
67. Hsu WY, Gierke TD. 1982. *Macromolecules* 15:101–5
68. Hsu WY, Gierke TD. 1983. *J. Membr. Sci.* 13:307–26
69. Deleted in proof
70. Starkweather HW Jr. 1982. *Macromolecules* 15:320–23
71. Litt MH. 1997. *Polymer Preprints* 38:80–81
72. Rebrov AV, Ozerin AN, Svergun DI, Bobrova LP, Bakeyev NF. 1990. *Polymer Sci. USSR* 32:1515–21
73. Krueger JJ. 2000. *Microstructural phase behavior in perfluorosulphonated ionomers.* PhD Diss. Univ. South Carolina. 99 pp.
74. Krueger JJ, Simon PP, Ploehn HJ. 2002. *Macromolecules* 35:5630–39
75. Khalatur PG, Talitskikh SK, Khokhlov AR. 2002. *Macromol. Theory Simul.* 11: 566–86
76. Ise M. 2000. *Polymer-Elektrolyt-Membranen: Untersuchungen zur Mikrostruktur und zu den Transporteigenschaften für Protonen und Wasser*. PhD thesis. Univ. Stuttgart. 177 pp.
77. Israelachvili JN. 1992. *Intermolecular and Surface Forces*. New York: Academic. 450 pp.
78. Bruni F, Ricci MA, Soper AK. 1998. *J. Chem. Phys.* 109:1478–85
79. Hartnig C, Witschel W, Spohr E. 1998. *J. Phys. Chem. B* 102:1241–49
80. Senapati S, Chandra A. 1999. *J. Chem. Phys.* 111:1223–30
81. Senapati S, Chandra A. 2001. *J. Phys. Chem. B* 105:5106–9
82. Brubach JB, Mermet A, Filabozzi A, Gerschel A, Lairez D, et al. 2001. *J. Phys. Chem. B.* 105:430–35
83. Gallo P, Ricci MA, Rovere M. 2002. *J. Chem. Phys.* 116:342–46
84. Paul R, Paddison SJ. 2001. In *Advances in Materials Theory and Modeling-Bridging Over Multiple-Length and Time Scales*, ed. V Bulatov, L Colombo, F Cleri, LJ Lewis, N Mousseau, pp. AA7.16.1–7.16.7. Warrendale, PA: Mater. Res.Soc.
85. Paul R, Paddison SJ. 2001. *J. Chem. Phys.* 115:7762–71
86. Paddison SJ, Paul R. 2003. *Solid State Ionics.* Submitted
87. Booth F. 1950. *J. Chem. Phys.* 19:391–94
88. Yam R, Nachliel E, Kiryati S, Gutman M, Huppert D. 1991. *Biophys. J.* 59:4–11
89. Gutman M, Nachliel E, Kiryati S. 1992. *Biophys. J.* 63:281–90
90. Shimoni E, Tsfadia Y, Nachliel E, Gutman M. 1993. *Biophys. J.* 643:472–79
91. Kotlyar AB, Borovok N, Kiryati S, Nachliel E, Gutman M. 1994. *Biochemistry* 33:873–79
92. Agmon N. 1995. *Chem. Phys. Lett.* 244: 456–62
93. Agmon N. 1995. *J. Mol. Liquids* 64:161–95
94. Kreuer KD. 1997. *Chem. Mater.* 8:610–41
95. Kreuer KD. 2000. *Solid State Ionics* 136–137:149–60
96. Tuckerman M, Laasonen K, Sprik M, Parrinello M. 1995. *J. Phys. Chem.* 99:5749–52
97. Tuckerman M, Laasonen K, Sprik M, Parrinello M. 1995. *J. Chem. Phys.* 103:150–61
98. Tuckerman ME, Marx D, Klein ML, Parrinello M. 1997. *Science* 275:817–20
99. Marx D, Tuckerman ME, Hutter J, Parrinello M. 1999. *Nature* 397:601–4
100. Marx D, Tuckerman ME, Parrinello M. 2000. *J. Phys. Condens. Matter* 12:A153–59
101. Paddison SJ, Pratt LR, Zawodzinski TA Jr, Reagor DW. 1998. *Fluid Phase Equilibria* 150–151:235–43
102. Paddison SJ, Zawodzinski TA Jr. 1998. *Solid State Ionics* 113–115:333–40
103. Paddison SJ, Pratt LR, Zawodzinski TA Jr. 1999. *J. New Mater. Electrochem. Syst.* 2:183–88
104. Paddison SJ, Pratt LR, Zawodzinski TA Jr. 1999. In *Proton Conducting Membrane Fuel Cells II*, ed. S Gottesfeld, TF

Fuller, pp. 99–105. Pennington, NY: Electrochem. Soc.
105. Paddison SJ, Pratt LR, Zawodzinski TA Jr. 2001. *J. Phys. Chem. A* 105:6266–68
106. Paddison SJ. 2001. *J. New Mater. Electrochem. Syst.* 4:197–207
107. Eikerling M, Paddison SJ, Zawodzinski TA Jr. 2002. *J. New Mater. Electrochem. Syst.* 54:15–23
108. Paddison SJ. 2003. In *Handbook of Fuel Cell–Fundamentals, Technology and Applications*, ed. W Vielstich, H Gasteiger, A Lamm, pp. Cambridge, UK: Wiley & Sons. Vol. 3. In press
109. Paddison SJ. 2003. *Solid State Ionics.* Submitted
110. Frisch MJ, Trucks GW, Schlegel HB, Scuseria GE, Robb MA, et al. 1998. *Gaussian 98* (Revision A.9) Pittsburgh, PA: Gaussian
111. Schlegel HB. 1982. *J. Comp. Chem.* 3:214–18
112. Hariharan PC, Pople JA. 1973. *Theor. Chim. Acta* 28:213–20
113. Becke AD. *J. Chem. Phys.* 98:5648–52
114. Breneman CM, Wiberg KB. 1990. *J. Comp. Chem.*, 11:361–73
115. Pratt LR, Tawa GJ, Hummer G, Garcia AE, Corcelli SA. 1997. *Int. J. Quant. Chem.* 64:121–41
116. Vishnyakov A, Neimark AV. 2000. *J. Phys. Chem. B* 104:4471–78
117. Vishnyakov A, Neimark AV. 2001. *J. Phys. Chem. B* 105:7830–34
118. Gottesfeld S, Zawodzinski TA. 1998. In *Advances in Electrochemical Science and Engineering*, ed. RC Alkire, H Gerischer, DM Kolb, CW Tobias, 5:197. Zurich: VCH
119. Paddison SJ. 2003. *J. Phys. Chem. B.* In press
120. Eikerling M, Paddison SJ, Pratt LR, Zawodzinski TA Jr. 2003. *Chem. Phys. Lett.* 368:108–14
121. Paddison SJ, Pratt LR, Zawodzinski TA Jr. 2003. *Mol. Phys.* Submitted
122. Spencer JB, Lundgren J-O. 1973. *Acta Cryst.* B29:1923–28
123. Cappadonia M, Erning JW, Saberi-Niaki SM, Stimming U. 1995. *Solid State Ionics* 77:65–69
124. Breslau BR, Miller IF. 1971. *Ind. Eng. Chem. Fundam.* 10:554–65
125. Capeci SW, Pintauro PN, Bennion DN. 1989. *J. Electrochem. Soc.* 136:2876–82
126. Verbrugge MW, Hill RF. 1990. *J. Electrochem. Soc.* 137:886–93
127. Pintauro PN, Verbrugge MW. 1989. *J. Membr. Sci.* 44:197–212
128. Bontha JR, Pintauro PN. 1994. *Chem. Eng. Sci.* 49:3835–51
129. Eikerling M, Kornyshev AA, Stimming U. 1997. *J. Phys. Chem. B* 101:10807–20
130. Eikerling M, Kornyshev AA, Kuznetsov AM, Ulstrup J, Walbran S. 2001. *J. Phys. Chem. B* 105:3646–62
131. Eikerling M, Kornyshev AA. 2001. *J. Electroanal. Chem.* 502:1–14
132. Corry B, Kuyucak S, Chung SH. 2000. *Chem. Phys. Lett.* 320:35–41
133. Din X.-D, Michaelides EE. 1998. *AIChE J.* 44:35–47
134. Paddison SJ, Paul R, Zawodzinski TA Jr. 1999. In *Proton Conducting Membrane Fuel Cells II*, ed. S Gottesfeld, TF Fuller, 98–27:106–20. Pennington, NJ: Electrochem. Soc. Proc. Ser.
135. Paddison SJ, Paul R, Zawodzinski TA Jr. 2000. *J. Electrochem. Soc.* 147:617–26
136. Paddison SJ, Paul R, Zawodzinski TA Jr. 2001. *J. Chem. Phys.* 115:7753–61
137. Paddison SJ, Paul R, Pivovar BS. 2001. In *Direct Methanol Fuel Cells*, ed. S Narayanan, S Gottesfeld, TA Zawodzinski, 01–014:8–13. Pennington, NJ: Electrochem. Soc. Proc. Ser.
138. Paddison SJ, Paul R, Kreuer KD, Zawodzinski TA Jr. 2001. In *Direct Methanol Fuel Cells*, ed. S Narayanan, S Gottesfeld, TA Zawodzinski, 01–04:29–33. Pennington, NJ: Electrochem. Soc. Proc. Ser.
139. Paddison SJ, Paul R, Kreuer KD. 2002. *Phys. Chem. Chem. Phys.* 4:1151–57
140. Paddison SJ, Paul R. 2002. *Phys. Chem. Chem. Phys.* 4:1158–63

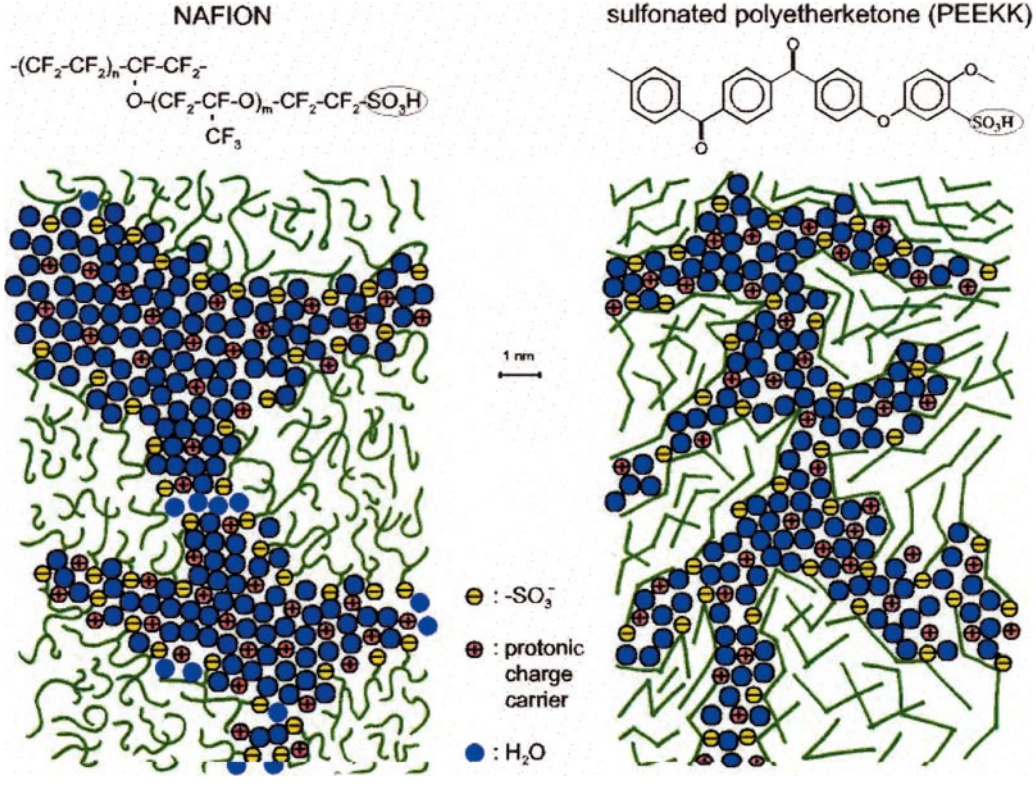

Figure 1 Schematic representation of the nano-phase separation in the hydrated morphology of Nafion and sulfonated PEEKK derived from experiments and modeling. This scheme illustrates the distinctions in the hydrophilic/hydrophobic separation, connectivity of the water and ion domains, and separation of the $-SO_3^-$ groups. Taken from Reference (6) with permission from Elsevier.

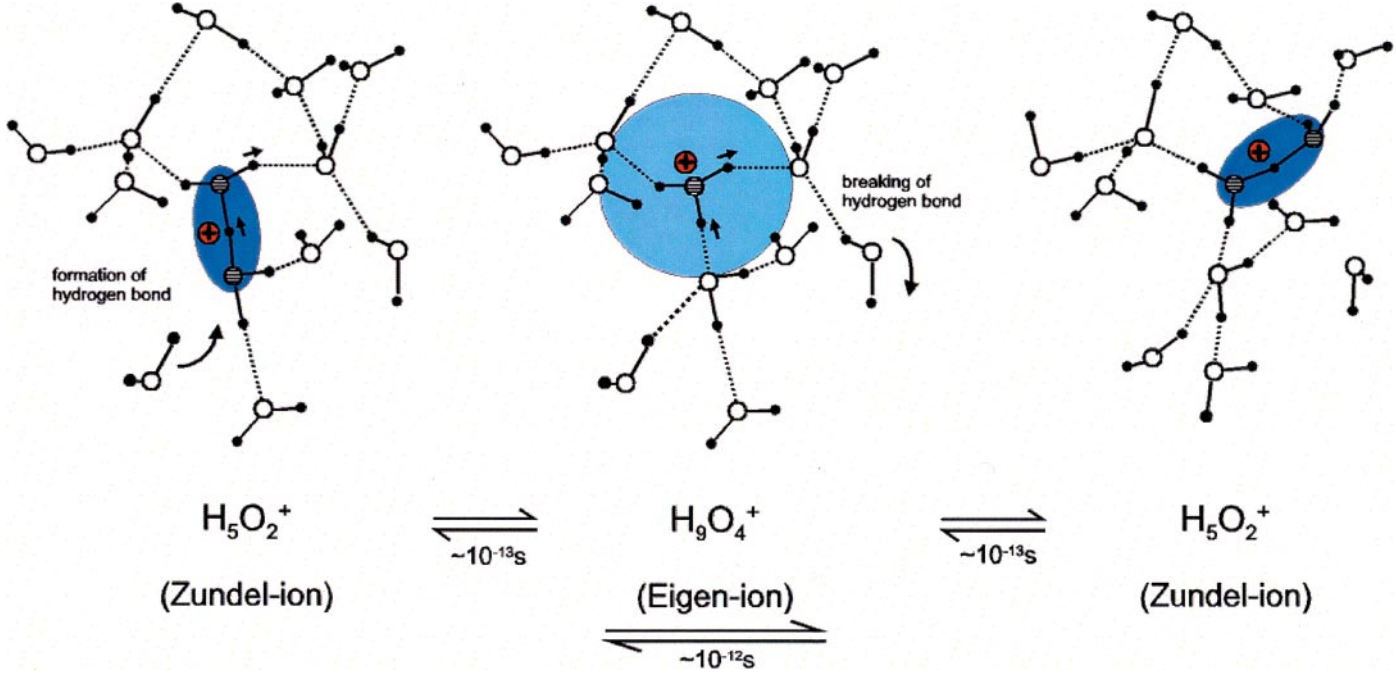

Figure 3 The proton transport mechanism in bulk water as conceived by the quantitative analysis of Kreuer (94, 95) and Agmon (92, 93) and the ab initio molecular dynamics simulations of Tuckerman (96–96) and Marx (99, 100). The regions where the hydrogen bonds are contracted are shown in blue. Important points to note include (*a*) the protonic charge follows the center of symmetry of the evolving hydrogen bond coordination, (*b*) the bond breaking and forming (reorientation) occurs in the weakly bound outer part of the complexes, (*c*) proton transfer occurs in the contracted central part of the complexes, and (*d*) there is a strong coupling of the processes in (*b*) and (*c*). Taken from Reference (95) with permission from Elsevier.

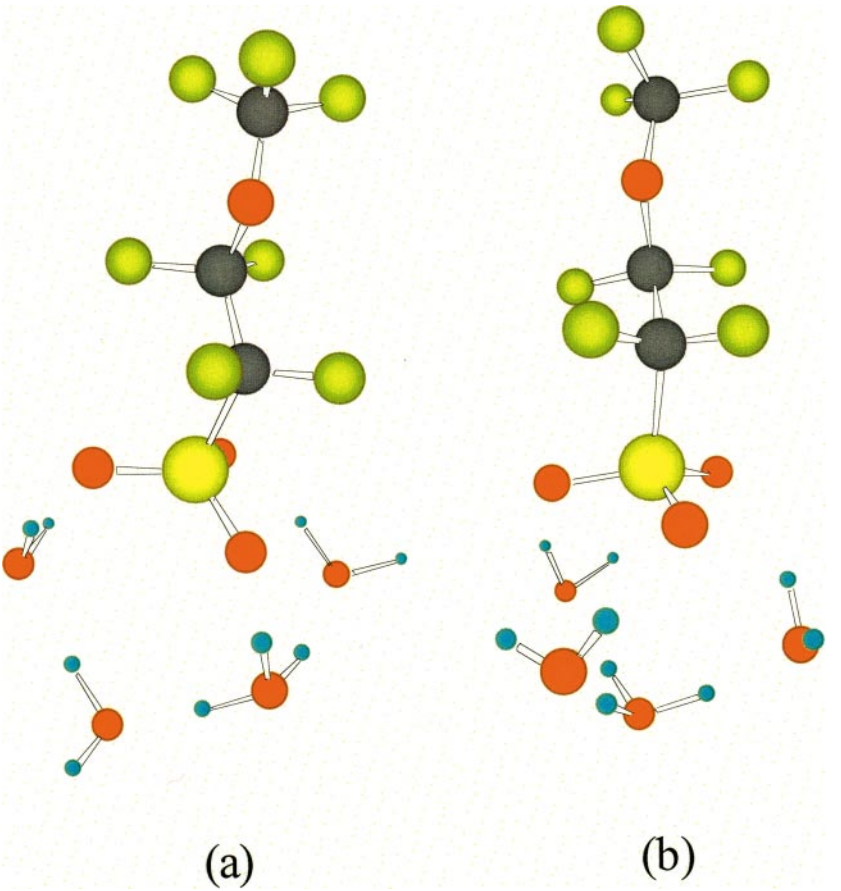

Figure 9 Fully optimized (B3LYP/6-31G**) conformations for clusters consisting of four water molecules with the Dow membrane short side chain. Note the distinction in the two structures. In (*a*) a contact ion pair as formed between the sulfonate anion and the hydronium ion, whereas in (*b*) the hydronium ion is separated from the anion with the network of an intermediate water layer. Of significance is the fact that structure (*b*) is favored over (*a*) in that it is 2.3 kcal/mol lower in energy.

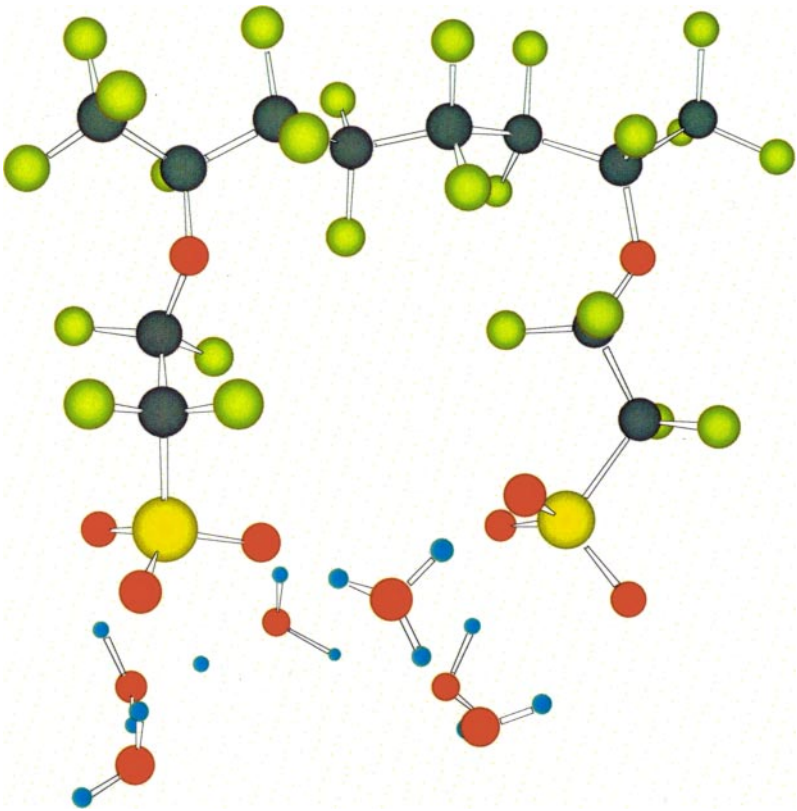

Figure 12 Minimum energy conformation (B3LYP/6-31G**) of the two-side chain fragment of the Dow PEM with six water molecules. This structure shows dissociation of both acidic protons: one as a hydronium ion hydrogen-bonded between the two sulfonate anions, and the other as a Zundel ion (a delocalized proton between two water molecules).